Contract No. 777564

INNOVATIVE RUNNING GEAR SOLUTIONS FOR NEW DEPENDABLE, SUSTAINABLE, INTELLIGENT AND COMFORTABLE RAIL VEHICLES

Deliverable 4.3 – Validation of complete virtual test method for structure-borne and airborne noise transmission

Due date of deliverable: 31/08/2019

Actual submission date: 20/09/2019

Leader/Responsible of this Deliverable: Pascal Bouvet, Vibratec

Reviewed: N

Document status		
Revision	Date	Description
1	30/8/19	First issue
2	17/9/19	After comments from TMT
3	20/9/19	Final version after TMT and quality check

This project has received funding from Shift2Rail Joint Undertaking under the European Union's Horizon 2020 research and innovation programme under grant agreement No 777564.

Dissemination Level		
PU	Public	X
CO	Confidential, restricted under conditions set out in Model Grant Agreement	
CI	Classified, information as referred to in Commission Decision 2001/844/EC	

Start date of project: 01/09/2017 Duration: 25 months

REPORT CONTRIBUTORS

Name	Company	Details of Contribution
Pascal Bouvet	Vibratec	Section 2, Section 4
Martin Rissmann	Vibratec	Section 2, Section 4
David Thompson	ISVR	Section 1, Section 3
Xiaowan Liu	ISVR	Section 3
Hui Li	ISVR	Section 3
Giacomo Squicciarini	ISVR	Section 3
Gang Xie	CDH	Section 2, Section 3.2

EXECUTIVE SUMMARY

This deliverable reports the results for noise transmission from the running gear to the train interior obtained with a virtual test method. The noise transmission is divided into structure-borne and airborne contributions. For each contribution results are compared to field measurements for validation.

For the prediction of the structure-borne noise contribution a new methodology has been developed covering the transmission from wheel rail-contact forces to interior noise, based on existing FE models of the running gear bogie including wheelsets and suspension elements. Acceleration levels and carbody forces are computed for unit wheel-rail contact loads, then subsequently post-processed with a newly developed algorithm in order to introduce operational conditions (roughness, speed, load, track receptance). Interior noise is obtained by multiplying the carbody forces with measured vibro-acoustic transfer functions to a receiver microphone. Comparisons with running measurements show satisfactory agreement such that the new methodology can be considered as validated and as being ready for industrial applications, notably since it represents a good compromise between accuracy and effort.

For the airborne sound prediction the noise radiated by the wheels, track and bogie frame and its transmission to the exterior sound pressure on the surface of the car body are predicted. The bogie frame noise radiation is assessed by the Boundary Element Method and results show that it can be neglected for interior/exterior noise. For the exterior sound pressure load on the carbody surface two separate models have been implemented: a Statistical Energy Analysis (SEA) model for the under-floor cavity and an original 2.5D boundary element model for the lateral sides. Finally, for the interior noise, an SEA model uses the exterior acoustic loading of the different panels (floor, doors, windows, lateral sides, gangway) and panel transmission (obtained from in situ measurements). Results of all intermediate steps have been validated by comparison with static and running tests.

Finally, the various models have been assembled and compared to measured noise levels. The following specific conclusions have been reached:

- Structure-borne noise:

  Is important up to 160 Hz for the investigated rolling stock. Generally, an accuracy of 1 to 3 dBA is reached. The agreement is very good between 80 and 400 Hz. Above this frequency the model under-predicts noise levels.

- Airborne noise:

  Is important between 100 and 5000 Hz for the investigated rolling stock. Generally, an accuracy of 2-3 dBA is achieved. Notably, due to particular features of the test track the model over-predicts the airborne contribution.

- Overall noise:

  Is dominated by the airborne noise in almost the entire frequency range, thus the accuracy is also 2-3 dBA.

- Methodologies

  Both methodologies used to assess noise contributions present a good compromise between accuracy and effort and may thus be of significant interest for rolling stock manufacturers.

The novel virtual test method will be used subsequently assessing novel noise reduction technologies for running gear.

ABBREVIATIONS AND ACRONYMS

ATV	Acoustic Transfer Vectors
BEM	Boundary Element Method
CAT	Corrugation Analysis Trolley
DOF	Degrees of Freedom
DPRS	Discrete Point Reacting Spring model
EMA	Experimental Modal Analysis
FEM	Finite Element Method
FRF	Frequency Response Function
RBE	Rigid Beam Element
SEA	Statistical Energy Analysis
SPC	Single Point Constraint
TDR	Track Decay Rate
TPA	Transfer Path Analysis
TSI	Technical Specifications for Interoperability
TWINS	Track-Wheel Interaction Noise Software

f	Frequency [Hz]
F	Force [N]
p	Pressure [Pa]
γ	Acceleration [m/s^2]
X	Longitudinal direction
Y	Lateral direction
Z	Vertical direction

TABLE OF CONTENTS

LIST OF FIGURES

LIST OF TABLES

1. INTRODUCTION

Workpackage 4 of RUN2Rail aims to develop tools and methodologies for predicting the transmission of noise and vibration from the running gear into the carbody and new technologies for reducing noise and vibration transmission in order to improve passenger comfort. In a previous step simulation models have been developed for predicting running gear noise that can be used as 'virtual test methods'. These have been described in Deliverable D4.2 [1].

In addition laboratory tests were carried out on various suspension elements (primary suspension spring, traction bar, lateral damper and associated bushings). Based on these measurements, models for the vibration transmission through these elements have been proposed. Results are reported in Deliverable D4.1 [2] and are used as input to the current model.

The work described in this report is focused on the validation of these models which have been integrated to form a versatile approach to modelling noise and vibration transmission through and from the bogie.

An extensive validation measurement campaign has been carried out for both static and running conditions in which noise and vibration at different locations have been recorded. The results are compared with predictions in this report.

The objectives of the work are to:

- Predict the structure-borne noise transmission by determining the wheelset vibration and developing simulation models for the vibration of the bogie frame. This gives the blocked forces (see Section 2.1) at the connection points on the car body.
- Determine the airborne noise transmission by predicting the noise radiated by the wheels, track and bogie frame and its transmission to the exterior sound pressure on the surface of the car body.
- Combine these two sub-models with measured transfer functions to obtain the noise inside the vehicle.
- Validate the modelling approach using the field measurements.

The work focuses on a trailer vehicle of a Metro de Madrid train. As it is a trailer vehicle, only rolling noise sources are considered. A series of static and running measurements have been performed on a test train for tuning the models and for their validation. The static measurements were described in Deliverable D4.2 [1]. The running measurements are described directly in this report when comparing predictions to measurements. A summary of measurement positions is given in the Appendix.

2. STRUCTURE-BORNE NOISE TRANSMISSION MODEL

The structure-borne path starts at the wheel/rail contact and propagates through the suspensions and bogie frame into the car body. For the chosen case study, the bogie frame has been modelled using Finite Elements (FE) and is coupled with models of primary and secondary suspension elements from D4.1 [2]. The blocked forces acting on the car body are predicted.

In order to assess the vibration levels at different points located on the bogie and the blocked forces under operational conditions, a post-processing step is applied to the FE results. Track dynamics based on analytical models (see sections 3.1.3 to 3.1.5), roughness excitation and contact filter are introduced. Finally, the structure-borne noise inside the vehicle is obtained by multiplying the calculated blocked forces with measured vibro-acoustic transfer functions p/F between the bogie-carbody connection point and interior microphones. The complete approach is described in detail in deliverable D4.2 [1].

The validation against measurements - carried out during a campaign in March 2018 at Metro de Madrid's Cuatro Vientos depot – covers vibration levels at the connection elements (see instrumentation plan in Appendix A.1), blocked forces and structure-borne interior noise. Measurements were carried out in static conditions as well as in dynamic conditions at about 50 km/h (see Table 1 for operational conditions). Results are compared in 1/3 octave bands between 50 and 1000 Hz with a focus on the region below 500 Hz where structure-borne noise is expected to be a more important contributor to interior noise. Concerning the validation one should keep in mind that the aim of this work is to demonstrate the viability of a new methodology to assess structure-borne noise in railway vehicles and not to reproduce perfectly the vehicle behaviour observed during the measurement. This would require a huge effort in terms of FE model tuning which is not in the scope of this project. Furthermore, parameters such as roughness and track dynamics contain some uncertainty due to the particular features of the depot track (e.g. sleeper spacing 1 m and ballast compaction).

Table 1: Operation conditions considered for structure-borne noise

Parameter	Value
Speed	54 km/h
Wheel load	3.6 tons/wheel
Roughness	Measured, refer to Figure 21
Track model	Continuously-supported model according to Table 5

2.1 MAIN RESULTS OF EXPERIMENTAL TPA

Structure-borne noise was assessed experimentally using path analysis (TPA) during the field tests in March 2018 at Metro de Madrid's Cuatro Vientos depot. The analysis to determine carbody forces was carried out with the so-called "in-situ blocked force method", which means without removing the traction bar and lateral damper elements during FRF measurements.

In order to determine operational blocked forces, the carbody connections were instrumented with accelerometers in all three coordinate directions X, Y, Z resulting in a force vector with 14 components (see Figure 1):

- traction bar: 2 sides x 3 directions = 6 force components (e.g. accelerometer 1320),
- lateral damper: 2 sides x 3 directions = 6 force components (e.g. accelerometer 1420),
- secondary suspension (not considered in the model since of second order): 1 side x 2 directions = 2 force components.

The blocked forces are estimated using an inverse method: the carbody accelerance matrix is measured, then inverted and combined with acceleration in operating conditions to estimate the blocked forces. Additional accelerometers, called indicators, are included in the analysis, e.g. 1322 & 1323 in Figure 1, to over-determine the system to be solved. In total the full input matrix consists of 14 forces x 28 indicators.

Figure 1: Carbody connection at the right side with accelerometers for TPA accelerance matrix

In the same way than computations, these measured blocked forces are then multiplied by measured vibro-acoustic transfer functions p/F of the carbody in order to estimate structure-borne noise contribution to interior noise levels. Figure 2 indicates the position of the interior microphones

used to evaluate structure-borne noise. This approach is quite common and referred to as a hybrid approach.

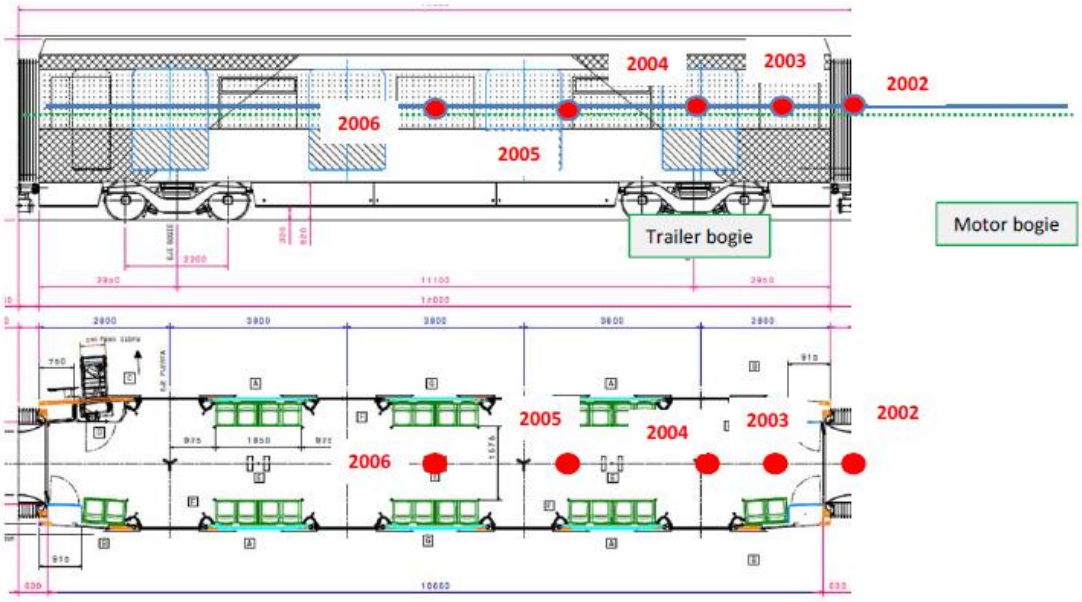

Figure 2: Interior microphone positions

From a qualitative point of view the experimental TPA revealed:

- The structure-borne contribution is dominant for microphones above the trailer bogie up to 160 Hz (see Figure 3). Above 400 Hz, structure-borne contribution is found at least 15 dBA below the total measured noise inside the vehicle: this indicates a clear predominance of airborne transmission.
- The main transfer paths are:
    - [80-100] Hz: traction bar in longitudinal direction X,
    - [125-315] Hz: traction bar in X and lateral damper in Y direction (lateral),
    - [400-500] Hz: lateral damper in Y direction (lateral).
- Inputs from the traction bar in the Y-direction can be neglected. The rubber bushing is very soft in this direction (shear motion).
- Inputs from the lateral damper in the X-direction can be neglected. The rubber bushing is very soft in this direction (shear motion).

- Inputs from the secondary suspension air spring are significantly lower than those from the traction bar and lateral damper.

Quantitative results of this TPA will be directly compared with simulated data in the following sections.

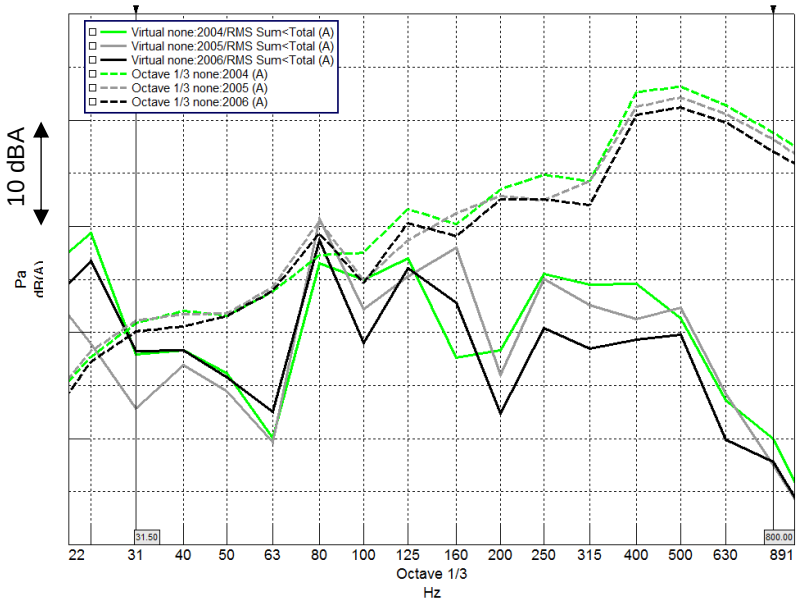

Figure 3: Structure-borne contribution to total interior noise for microphones 2004-2006 (based on experimental data)

2.2 FE MODELS OF BOGIE AND WHEELSETS

In this work package, a trailer bogie of a Metro Madrid vehicle is modelled using the FE package Nastran. The full FE model includes the bogie frame, a front wheelset, a rear wheelset, axle boxes, primary suspension springs, lateral dampers and traction bars, as shown in Figure 4. This also shows the global coordinate directions. The wheelsets, bogie frame and axle boxes are modelled using solid elements. The dampers and traction bars are modelled approximately using one-dimensional beam elements because the actual geometry data were not available. The primary suspension springs are modelled using spring-damper elements with the measured frequency-dependent properties from Deliverable D4.1 [2]. The numbers of elements are listed in Table 2. The FE bogie model consists of over 1.36 million nodes. This corresponds to a model size of about 4 million degrees of freedom (DOF), which is nowadays a medium size FE model for dynamic computation.

Table 2: FE model information

	Wheelsets	Bogie frame	Primary springs	Traction bars	Lateral dampers
Nodes	163,956	1,205,380	32	4	4
Elements					
Tetra	87,438	61,5254	-	-	-
Bush	16	-	8	4	4
Mass	12	-	16	-	-
Beam	-	-	-	4	4
RBE	32	8	16	-	-
SPC	-	-	-	2	2

A constant damping loss factor of 0.08 was applied to the FE model after correlating the calculated responses with the static measurements described in Deliverable D4.2. The frequency-dependent stiffness of bushing elements for traction bars and lateral dampers were not used initially, being replaced with constant stiffness values as listed in Table 3.

Table 3: Stiffnesses of bushing elements

Global coordinate direction	Lateral damper (MN/m)	Traction bar (MN/m)
X	5	10
Y	20	2
Z	20	10

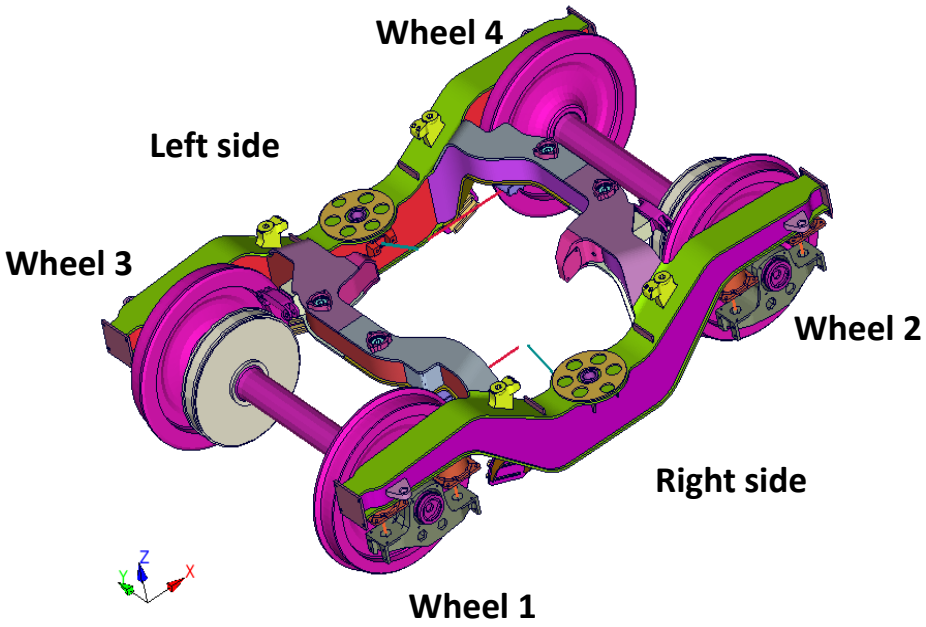

Figure 4. FE model of the trailer bogie

2.3 CONTACT FORCES

Figure 5 shows the computed vertical and lateral contact forces obtained for roughness excitation after applying the contact filter. Due to the out-of-centre position of the brake discs on the axle, contact forces for the two wheels of the same axle are slightly different. The impact on the lateral direction is stronger, probably due to axle bending modes.

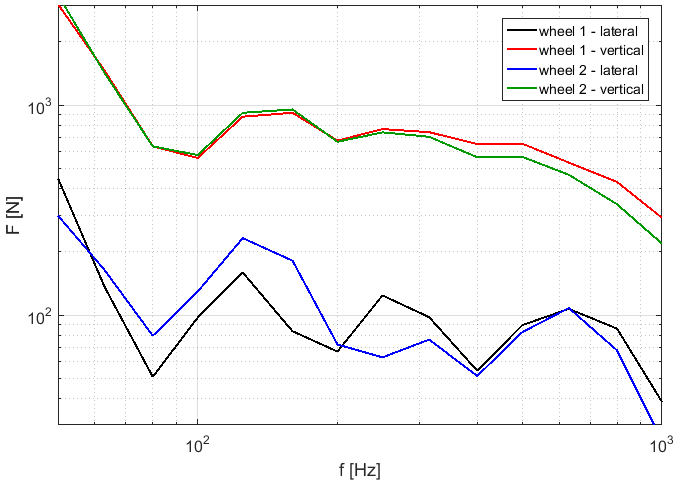

Figure 5: Contact forces for filtered roughness excitation – wheel 1 (furthest to the disc) & 2 (nearest from the disc)

2.4 COMPARISON OF VIBRATION AT CONNECTION ELEMENTS

In order to validate the numerical approach, vibration levels at the connection elements are compared with measurements obtained from dynamic tests. For simplicity only the main transfer directions are considered.

2.4.1 Axlebox

Figure 6 shows the vertical axlebox acceleration. Generally the order of magnitude and spectrum shape obtained with the numerical model is satisfactory. The levels are over-predicted by roughly 10 dB between 125 and 400 Hz; below 100 Hz the prediction is less satisfactory. Reasons could be uncertainties related to the measured rail roughness, track impedance or to a lesser extent other sources such as the use of a constant global damping value in the model.

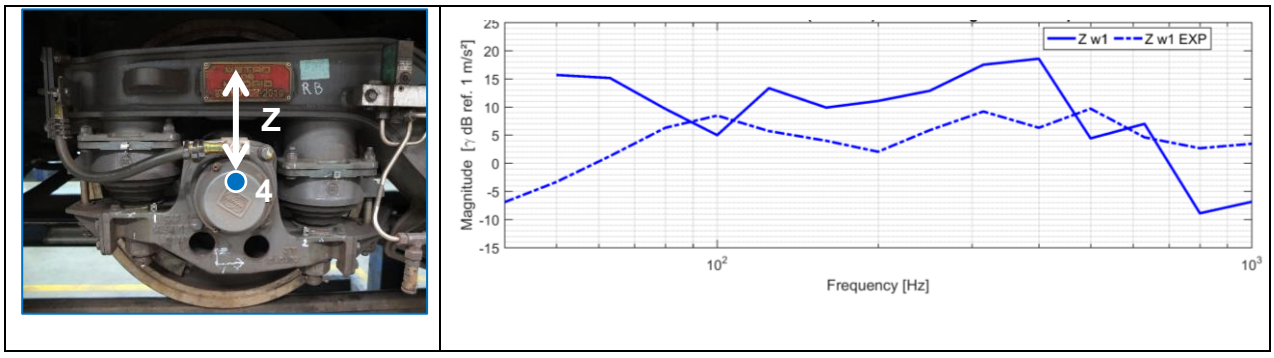

Figure 6: Acceleration levels at the axlebox of wheel 1 – measurements (-··-)

2.4.2 Primary suspension

Figure 7 and Figure 8 show vertical acceleration levels at positions either side of one primary suspension element of wheel 1 and wheel 3: the upstream side, i.e. nearest the wheelset (black) and the downstream side, i.e. on the bogie frame (red). Note that frequency-dependent stiffness as reported in deliverable D4.1 [2] is used in the model. For wheel 1 (furthest from the disc) the order of magnitude, level of isolation (20 to 30 dB) and spectrum shape obtained with the numerical model are satisfactory. Discrepancies observed at the axlebox (Figure 6) are transmitted to the upstream position of the primary suspension. Concerning the downstream accelerations, a small underestimation is observed. For wheel 3 (opposite of wheel 1, nearest to the disc) upstream levels are overestimated by approximately 15 dB (but similar to predictions of wheel 1), however downstream levels agree well. Thus the bogie input vibration relevant to structure-borne noise is predicted with good quality for both wheels.

Finally, note that in both cases, the computations tend to overestimate the vibration filtering by the rubber mounts.

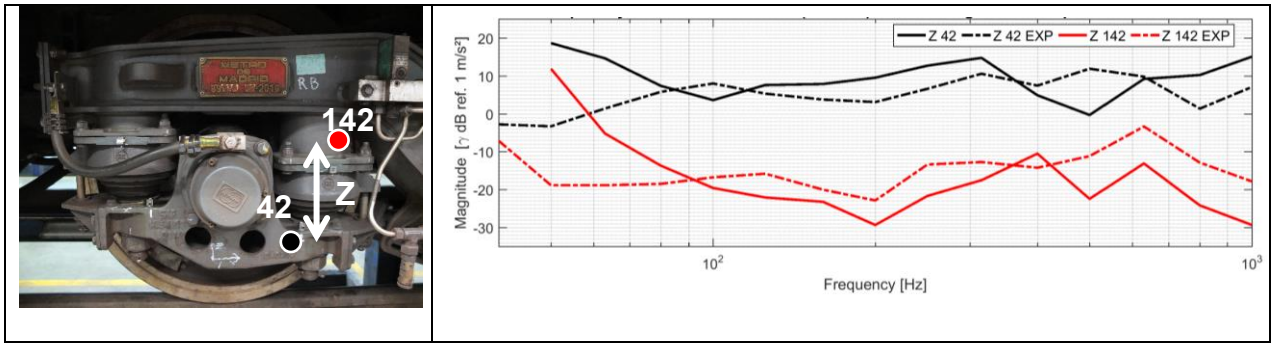

Figure 7: Acceleration levels in vertical direction Z at the primary suspension of wheel 1 (furthest to the disc) – measurements (-··-)

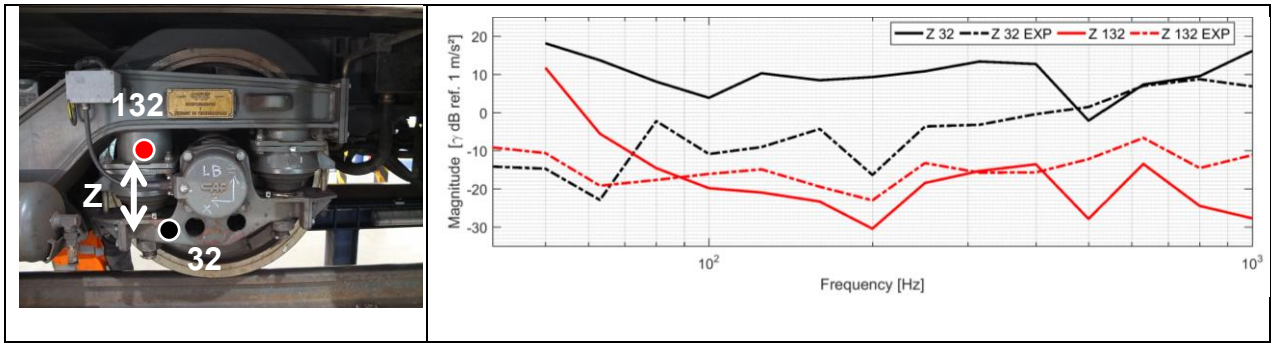

Figure 8: Acceleration levels in vertical direction Z at the primary suspension of wheel 3 (opposite of wheel 1 – nearest from the disc) – measurements (-··-)

2.4.3 Traction bar

Figure 9 shows the acceleration levels in the longitudinal direction (X in gobal coordinates) of the right traction bar (between wheels 1 & 2). The upstream position is located on the bogie (black) and the downstream position (red) is located directly after the bushing on the traction bar. Note that constant stiffness values are used (Table 3). Comparison of the upstream position is generally satisfactory bearing in mind that discrepancies for components further upstream are transmitted. However, for the downstream position the agreement is only acceptable up to 200 Hz; above that, the levels are strongly under-predicted indicating that the vibration filtering by the rubber mounts is overestimated.

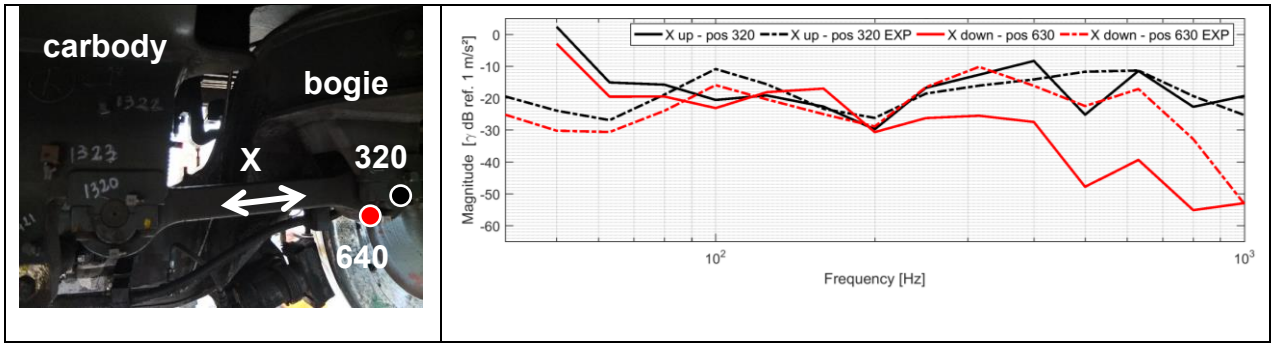

Figure 9: Acceleration levels in longitudinal direction X at the traction bar on the right side (wheels 1 & 2) – measurements (-··-)

2.4.4 Lateral damper

Figure 10 shows the acceleration levels in the longitudinal direction (Y in global coordinates) of the right lateral damper between wheels 1 & 2. The upstream position is located on the bogie (black) and the downstream position (red) is located directly after the bushing on the damper. Note that constant stiffness values are used (Table 3). Comparison of the upstream position is generally satisfactory having in mind that discrepancies of further upstream components are transmitted. However, here again the model predicts a significant vibration filtering by the rubber bushings above 500 Hz, whereas no filtering is observed in the measurements.

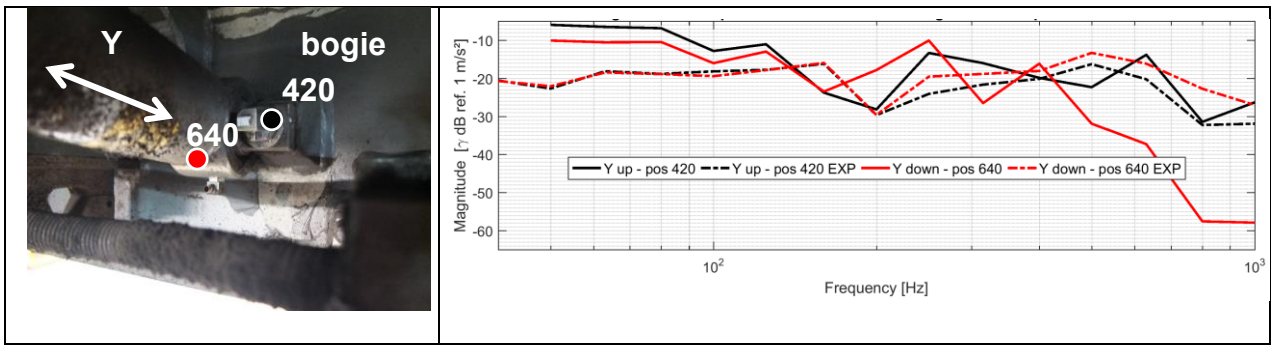

Figure 10: Acceleration levels in lateral direction at the lateral damper on the right side (wheels 1 & 2) – measurements (-·-)

2.5 COMPARISON OF BLOCKED FORCES

Figure 11 compares the main contributing blocked forces of the right traction bar (wheels 1 & 2). In the longitudinal (X) direction the order of magnitude and shape fit well up to 200 Hz; at higher frequencies under-estimation is observed.

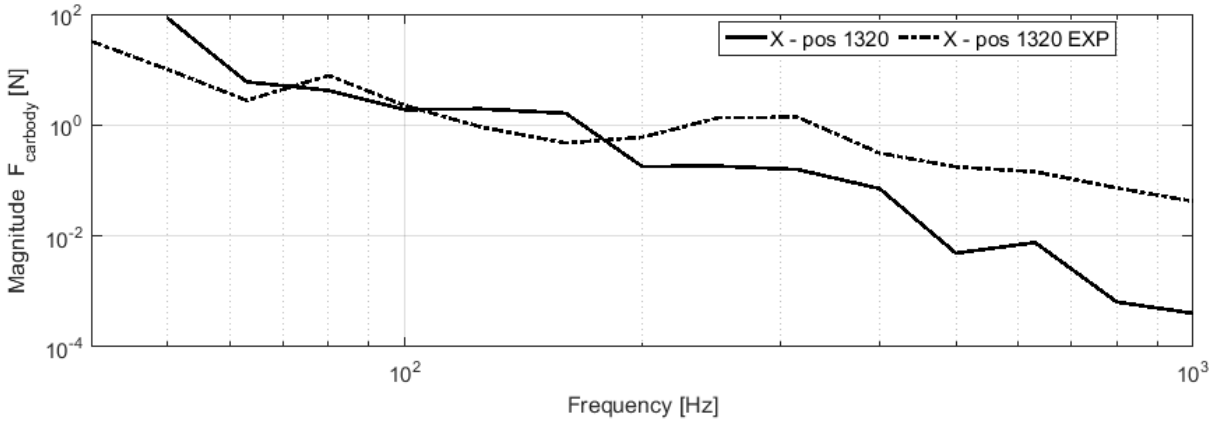

Figure 11: Main contributing blocked forces of the traction bar: predictions (–) measurements (-·-)

Figure 12 compares the main contributing blocked forces of the right lateral damper (wheels 1 & 2). In the lateral (Y) direction the order of magnitude and shape fit well up to 400 Hz; above this frequency under-estimation is observed. In the vertical (Z) direction the model overestimates up to 250 Hz, agrees well up to 500 Hz and then underestimates strongly. Generally, the prediction for the lateral damper is more satisfactory than that for the traction bar.

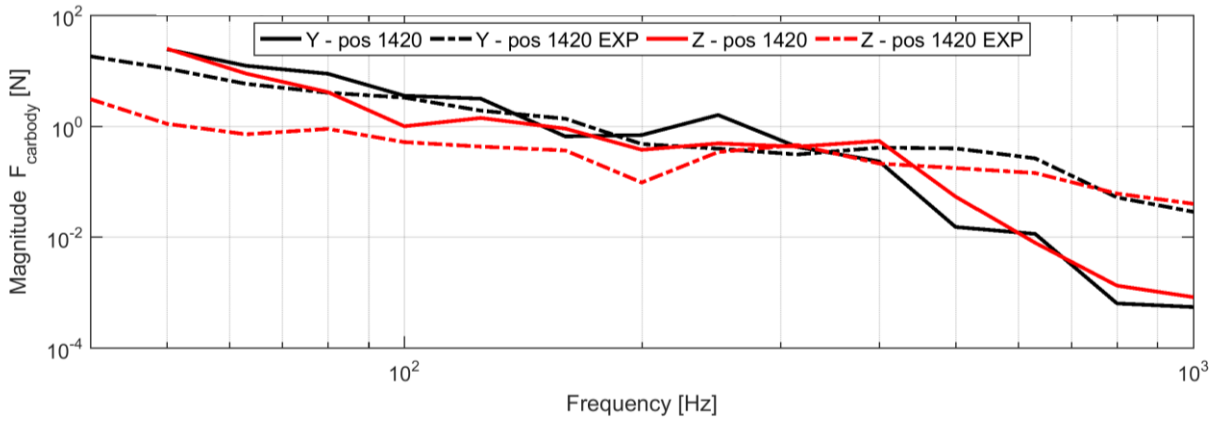

Figure 12: Main contributing blocked forces of the lateral damper: predictions (–) measurements (-•-)

2.6 STRUCTURE-BORNE NOISE INSIDE THE VEHICLE

2.6.1 Vibroacoustic transfer function p/F

The simulation model used for structure-borne noise does not include the carbody (not available in this project). Therefore the structure-borne sound inside the vehicle is estimated by using a hybrid approach. Blocked forces are calculated with the model and multiplied with experimentally determined vibro-acoustic transfer functions p/F.

The measured vibro-acoustic transfer function p/F for one of the two lateral damper attachment points at the carbody is illustrated in Figure 13. On the right, transfer functions p/F to an interior microphone located in the centre above the investigated bogie are shown by way of example for the main directions of the traction bar (X, axial to the bar) and the lateral damper (Y, axial to the damper). For simplicity the average transfer functions of the traction bars and the lateral dampers of both bogie sides are presented.

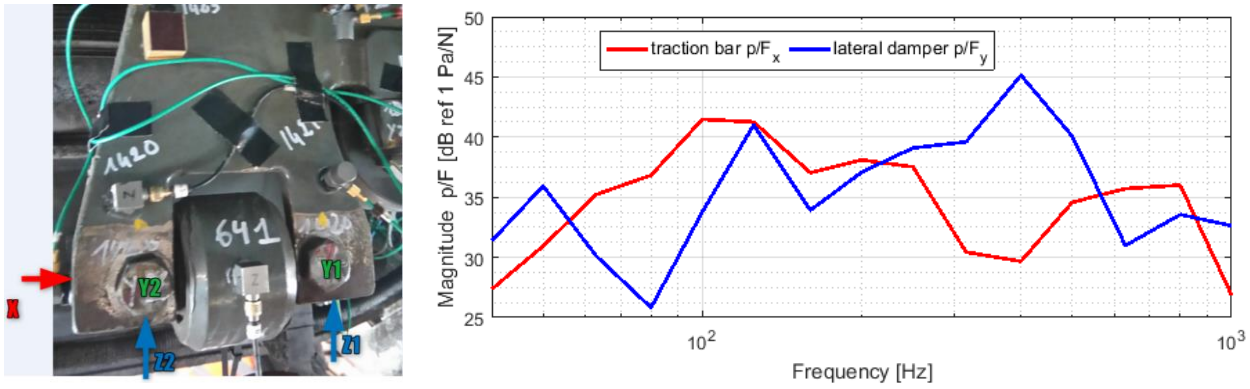

Figure 13: Measurement location (left, lateral damper) and vibroacoustic transfer function p/F (right) in the main direction of the traction bar and lateral damper

2.6.2 Structure-borne noise levels

Figure 14 compares the structure-borne noise contribution at one microphone position inside the vehicle, above a trailer bogie. A very satisfactory agreement is observed between 80 and 400 Hz, which corresponds to the frequency range for which structure-borne noise was found to be significant during tests.

At low frequencies (below 50 Hz), discrepancies could be related to the measured rail roughness or track impedance.

Above 500 Hz, the computations under-estimate the structure-borne noise contribution: as shown in previous sections, this is likely to be due to the over-estimation of the filtration effect by the rubber

bushings at the extremities of the lateral dampers and traction bars. Blocked forces (Figure 11 and Figure 12) and thus structure-borne noise are then under-estimated compared with the measured estimates.

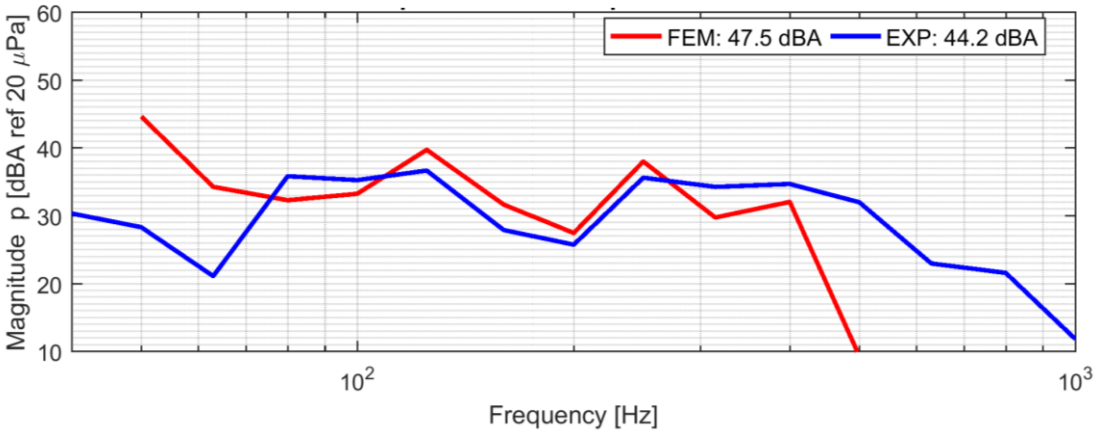

Figure 14: Comparison of structure-borne noise levels inside the vehicle (microphone 2004)

Figure 15 shows the structure-borne noise contributions of the traction bar and the lateral damper as well as the overall level. The prediction of the main transfer path agrees qualitatively with the experimental TPA. The contribution of the traction bar is predicted to be much lower than the measurement above 200 Hz. However one has to keep in mind that for the case study here the structure-borne noise is an only important contributor to the overall noise up to 160 Hz (see Figure 3).

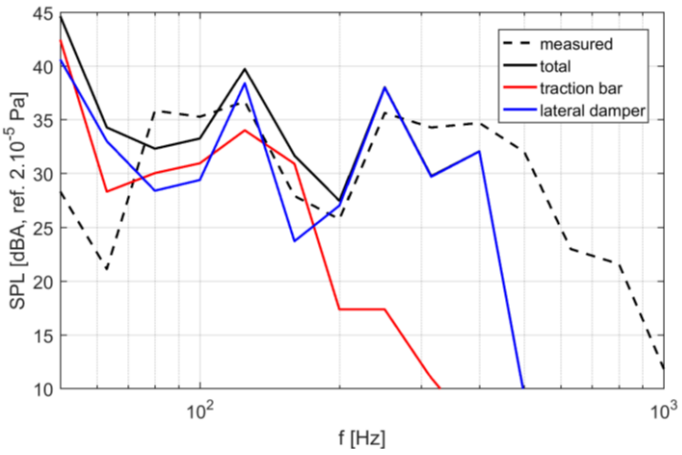

Figure 15: Structure-borne noise contributions (microphone 2004)

Table 4 presents a comparison of global structure-borne noise levels obtained from TPA tests and computations: here again the comparison is very satisfactory. Looking more in detail at the relative contribution of each transfer path it appears that:

- Between [80-100] Hz: TPA tests and computations shows that the traction bar in the X direction (longitudinal) is the dominant path,
- Between [125-315] Hz: TPA tests show that the traction bars in X (longitudinal) and the lateral dampers in Y direction (lateral) are dominant paths. Computations are in agreement for the dampers, but the traction bar is found to be significant only up to 200 Hz.
- Between [400-500] Hz: TPA tests and computations shows that the lateral dampers in Y direction (lateral) is the dominant path.

Table 4: Structure-borne noise levels inside the vehicle (microphone 2004)

Frequency range [Hz]	Total [dBA]		Traction bar [dBA]	Lateral damper [dBA]
	FEM	EXP	FEM	FEM
50 – 1000	47.5	44.0	43.9	45.0
80 – 400	43.9	43.5	37.9	42.6

2.7 PARAMETER VARIATIONS

Parametric studies have been considered with the numerical model, aiming at testing the sensitivity of interior noise levels to various track parameters and roughness.

2.7.1 Increased ballast stiffness & corrected roughness

Predictions from the reference model are too high by 10 to 20 dB for frequencies below 100 Hz. Reasons for this could be errors in the rail roughness data, notably for long wavelengths (limitation of the measuring system) and low frequency track dynamics. Actually, the track model presented in Section 3.1 is based on measurements on the track in unloaded conditions. However, it is known that dynamic ballast stiffness could be higher for a loaded track. In order to study those effects a corrected rail roughness is used (based on a fit of rail vibration levels) and the ballast stiffness is increased by a factor of 2 for the track model. The results are shown in Figure 16. Globally, structure-borne noise is now under-predicted. However, the trend of the measured curve is better captured below 80 Hz. These results outline the particular sensitivity of the structure-borne noise

model to track dynamics and roughness levels. Consequently, high quality data for these parameters is essential for accurate noise level predictions. Nevertheless, the model can still be used to study relative changes in structure-borne noise.

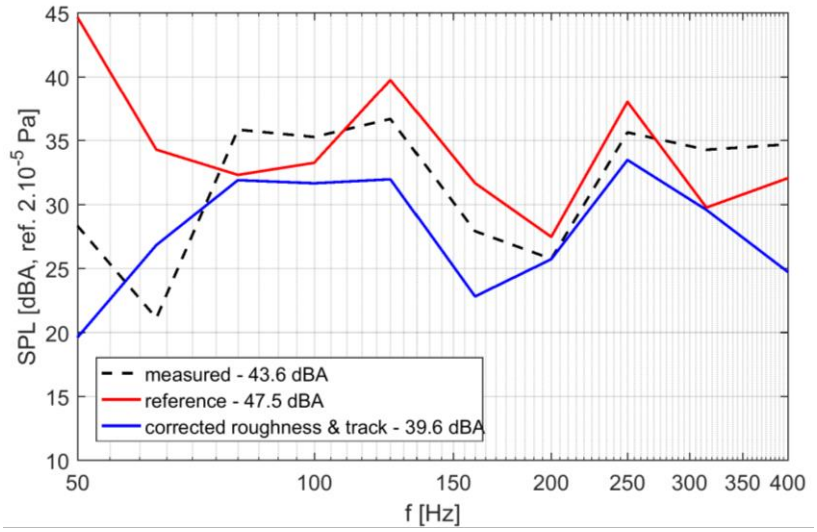

Figure 16: Structure-borne noise for corrected roughness & track dynamics (microphone 2004)

2.7.2 Continuous track vs. discrete track model

For the validation process of the structure-borne noise model a continuously supported track model is used. Figure 17 shows the structure-borne noise levels and spectra for the discretely supported track model as described in Section 3.1. Both configurations considered, for wheel-rail contact over a sleeper (above) and at midspan, lead to higher noise levels. The spectral shape is equivalent, except for frequencies above 300 Hz, where the discrete model covers the pinned-pinned frequency and is thus closer to the measurements.

In this case, the track model has a significant effect on the track receptance and thus on structure-borne noise. This effect is probably related to the large sleeper spacing (1 m) at the test track, which induces a low frequency of the first pinned-pinned mode. With more conventional sleeper spacing (typically 0.6 m) it is likely that the effect of the track model on structure-borne noise predictions will be lower.

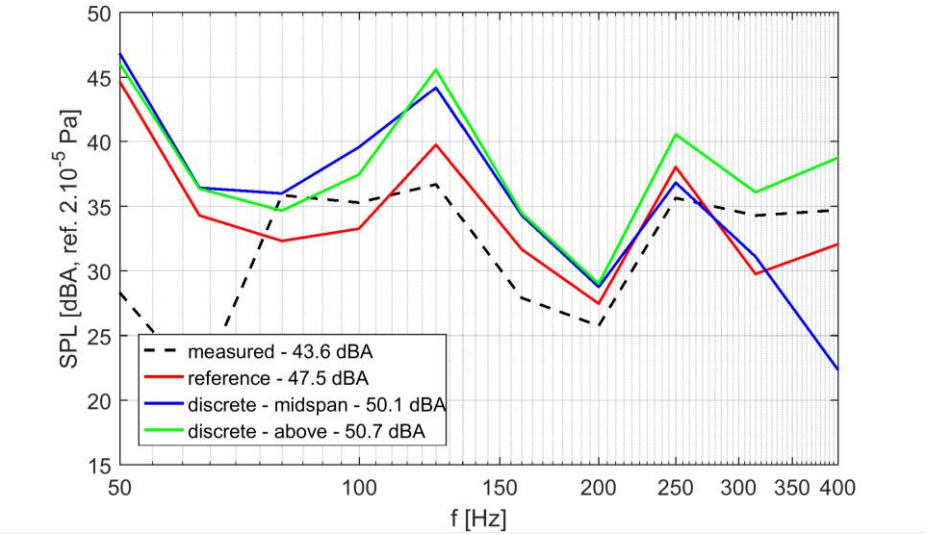

Figure 17: Structure-borne noise for different track models (reference with continuous beam model, microphone 2004).

3. AIRBORNE NOISE TRANSMISSION MODEL

In the airborne path sound starts from the wheel and track vibration and propagates through the air until it reaches the external boundary of the car body. The model for the airborne propagation path is described in this section. Noise radiated from the vibrating wheels, rail and sleepers is predicted using TWINS [3]. In addition the noise radiated by the bogie is predicted using the bogie model from the previous section. The noise propagates through the air underneath the car body where it develops a partially diffuse field. An SEA model of the under-floor cavity has been developed to obtain sound pressure levels at the train floor. Through reflections and diffraction, noise also reaches the sides of the train and can enter the car body through the side walls, windows, doors and gangways. A 2.5D boundary element model is used for this. The sound transmitted to the interior will be determined using measured data for the sound transmission loss of the vehicle floor, walls, etc.

3.1 ROLLING NOISE

3.1.1 Introduction

This section presents comparisons between the TWINS predictions and the measured results in terms of track decay rate, rail mobility, rail and sleeper vibration and noise radiation. In the predictions, a discretely supported track model has been implemented. Based on the remaining difference between the predicted and measured vibration, a correction is determined and applied to the predicted noise results. The corrected sound power is used in the subsequent noise transmission calculations.

3.1.2 Background

The track system consists of rails, pads, sleepers and ballast and is modelled by a Timoshenko beam model with two-layer support, as shown in Figure 18. The support is often modelled as continuous. However, in the current measurements, the sleeper spacing is large (1 m), and the rail pads have a high value of stiffness. Consequently, significant differences are found between the rail response measured above a sleeper and at mid-span. The effect of the discrete support provided by the sleepers is therefore considered. The response in the discretely supported model is determined from the superposition of the response of the rail to the contact force and the response to the reaction forces at each support point [4].

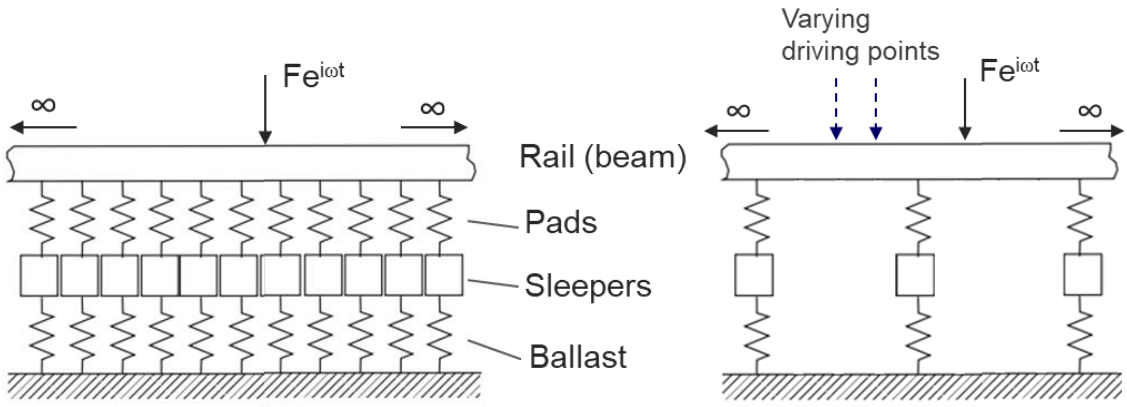

Figure 18: Models for track vibration: (a) continuously supported; (b) discretely supported [3].

For the discretely supported model, the rail behaviour within a sleeper span varies according to the position of the driving point. Calculations are carried out for three different excitation positions, above a sleeper, quarter-span and mid-span. The vibration and noise results are then determined by taking the average over different excitation positions.

The parameters used in the models are listed in Table 5. These have been determined in order to obtain the best fit between the predictions and the measurements of mobility and decay rate described in the next sections.

Table 5: Parameters used for the track

	Vertical	Lateral
Rail bending stiffness (Nm^2)	4.84×10^6	0.88×10^6
Rail shear coefficient	0.5	0.5
Rail loss factor	0.02	0.02
Mass per length (kg/m)	54	
Cross receptance level (dB)	-7	
Pad stiffness (MN/m)	800	100
Pad loss factor	0.2	0.2
Sleeper mass (kg)	150	
Distance between sleepers (m)	1.0	
Ballast stiffness (MN/m)	100*	35
Ballast loss factor	1.0*	2.0

* frequency dependent

In the TWINS model used, the effect of the ground on the rail and sleeper radiation has been taken into account based on the work of Zhang et al. [5],[6].

3.1.3 Rail mobility

Figure 19(a) presents the measurements and predictions of the rail mobility above a sleeper; Figure 19(b) shows the corresponding results at mid-span. Predicted results are shown for both the continuously and discretely supported track models. There is a discontinuity in the measured mobility above the sleeper at 500 Hz. This is because the data below and above this frequency were obtained using different types of hammer. The first pinned-pinned mode occurs at 457 Hz, where a peak is found in the mobility at mid-span; the second one occurs at 1490 Hz which leads to a dip in the mobilities both at mid-span and above a sleeper. These phenomena are not seen in the continuously supported model, but are well predicted by the discrete one.

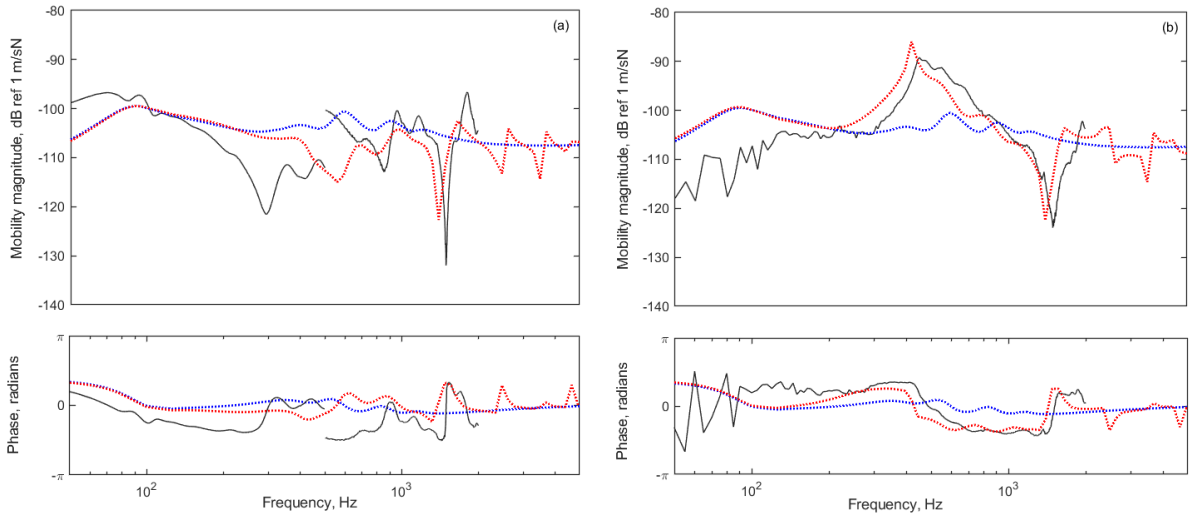

Figure 19: Rail point mobility (a) above a sleeper and (b) at mid-span. —, measurement; …, continuously supported model; …, discretely supported model.

3.1.4 Track decay rate

The measured and predicted track decay rates are compared in Figure 20 which also includes the limit curves from ISO 3095:2013 [7] for reference. The predicted results from the continuously and discretely supported track models are both presented. Appropriate pad stiffnesses are determined for each model, see also Table 1. The differences in vertical decay rate between the two models occur mainly around the first (457 Hz) and second (1490 Hz) pinned-pinned frequencies. The discretely supported model predicts a dip at 457 Hz and a peak at 1490 Hz, whereas these are not found in the continuous model. Similar phenomena are observed for the lateral direction at lower frequencies. In general, both models provide reasonable agreement with the measured results.

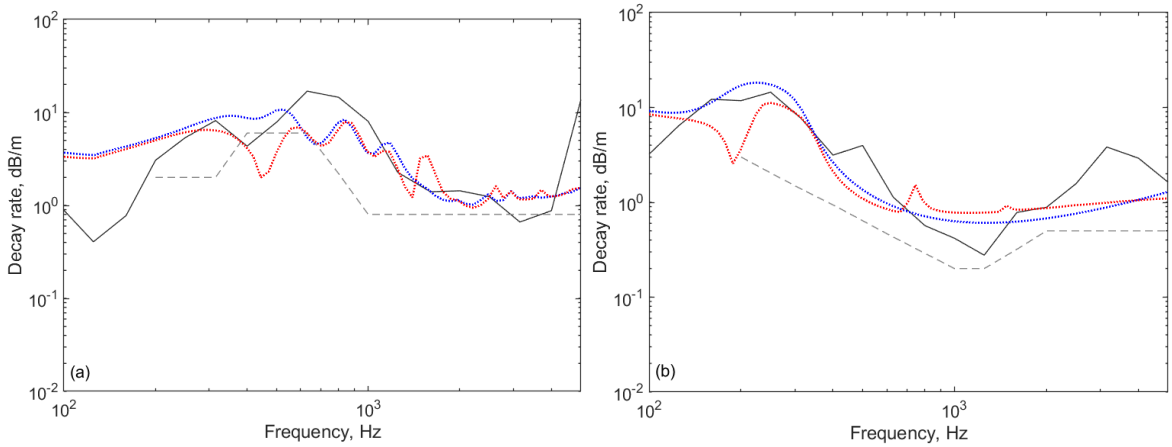

(a) (b)

Figure 20: Vertical (a) and lateral (b) track decay. - -, ISO 3095:2013 Limit; —, measurement; continuously supported model (pad stiffness: vertical 800 MN/m and lateral 156 MN/m); …, discretely supported model (pad stiffness: vertical 800 MN/m and lateral 100 MN/m).

3.1.5 Rail and sleeper vibration

To calculate the track vibration and noise, the roughness spectrum is required. Figure 21 shows the one-third octave band spectra of wheel and rail roughness which are used as input to the TWINS model. These are the averaged levels of the measured data described in D4.2 [1]. For the wheel, the average was taken over 4 trailer bogie wheels with 4 lines on each wheel; for the rail, it is averaged over the left and right rails with 5 lines on each. The limit spectrum from ISO 3095:2013 [7] (as used in the TSI-Noise) is also shown in Figure 21 for reference. The rail roughness is higher than the ISO limit curve and seems particularly high at long wavelengths, whereas the wheel roughness is generally much lower than the ISO limit.

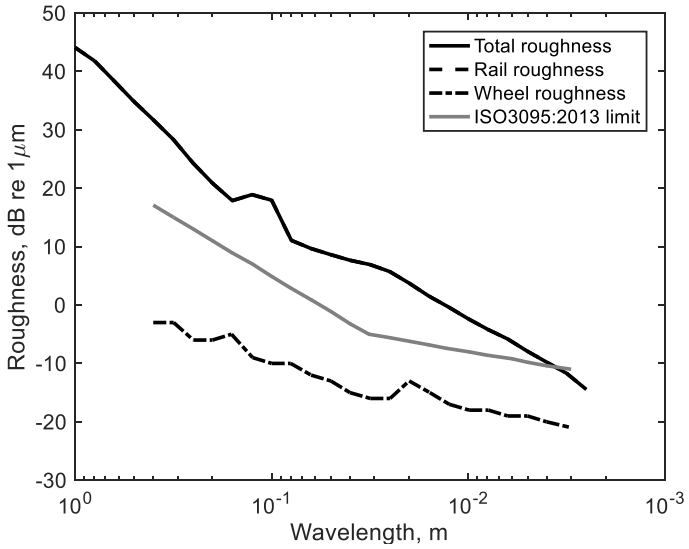

Figure 21: Wheel and rail roughness spectra

The vertical and lateral rail vibration during the train passage is presented in Figure 22 from both measurements and predictions. The predictions are based on the calculated decay rates. The measurement results are shown for response positions at mid-span and above a sleeper. Predicted results are shown from both the continuously and discretely supported track models. Compared with the measured vertical vibration, the results predicted using the continuously supported model are much lower between 200 and 1000 Hz. The levels are much improved by using the discretely supported model, although the predicted levels are still lower than the measured ones. The differences between the two locations obtained from the measurements and the discretely supported model are similar, as shown in Figure 23. In both cases the differences show a broad peak in the frequency range 200 – 1000 Hz with a maximum difference of approximately 10 dB. The improvements obtained by using the discretely supported model are smaller for the lateral direction.

Below 200 Hz the predicted vibration for both directions is more than 10 dB greater than the measurements. This suggests that the high values of rail roughness found at long wavelengths (greater than 0.1 m) in Figure 21 may be incorrect.

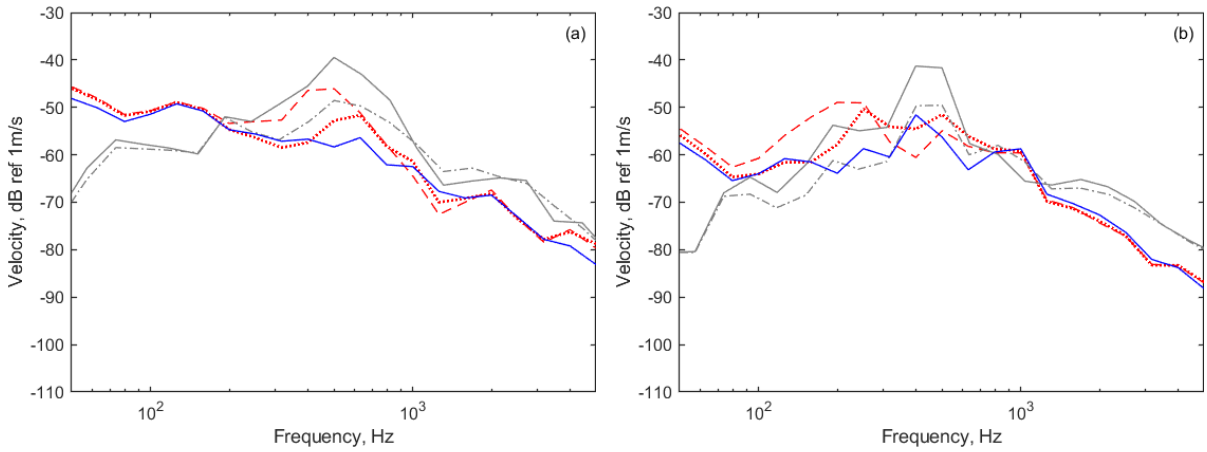

Figure 22: Rail vertical (a) and lateral (b) vibration at different locations during train pass-by. —, measurement at mid-span; -.-, measurement above sleeper; —, TWINS prediction with continuous support; - -, TWINS prediction with discrete supports at mid-span; …, TWINS prediction with discrete supports above sleeper.

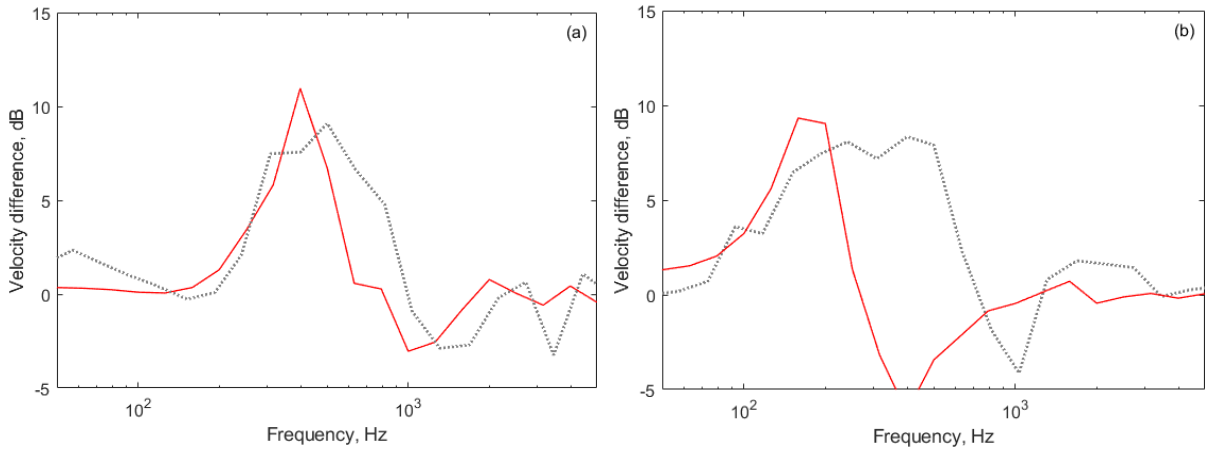

Figure 23: Difference in rail vertical (a) and lateral (b) vibration between above sleeper and at mid-span. …, measurement; …, TWINS prediction with discrete supports.

Figure 24 shows measured and predicted sleeper vibration during the train pass-by. In both models, the sleeper is considered as flexible. There is only a small difference between the results from the models with continuous and discrete support. Similar to the rail vibration, the levels are over-predicted below 200 Hz with differences of generally around 10 dB. Above 1250 Hz under-predictions are noticeable. Between 200 and 1250 Hz, the agreement is generally good with differences of less than 5 dB.

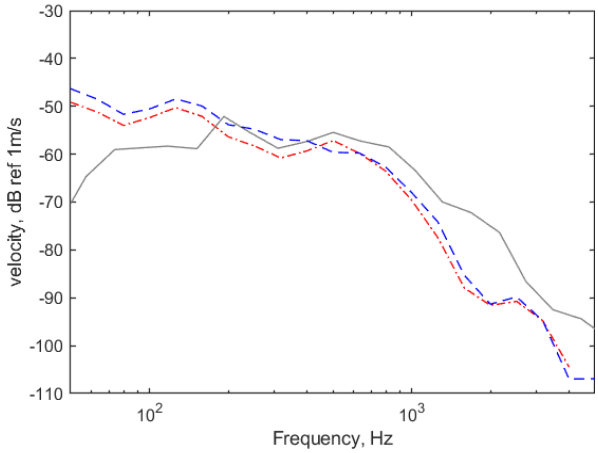

Figure 24: Sleeper vibration during train pass-by. —, measurement; - -, TWINS prediction with continuous support; -.-, TWINS prediction with discrete supports.

3.1.6 Noise radiation

The predicted A-weighted noise spectra are compared with the measured results in Figure 25. The measurement setups including the receiver locations are described in Appendix A.2. Figure 25(a) shows the average results for microphones M1 and M2 which are 4 m from the nearest rail (4.75 m from the track centreline) at heights of 1.4 and 2 m. Figure 25(b) shows results for microphone M3 which is at 7.5 m from the track centreline. The spectral trends are well predicted by both models, while the levels are generally lower in the predictions. Better agreement is obtained between 500 and 800 Hz by using the discretely supported model, which is consistent with the findings for the rail vibration. The deviations from the measurements are more obvious for receiver M3.

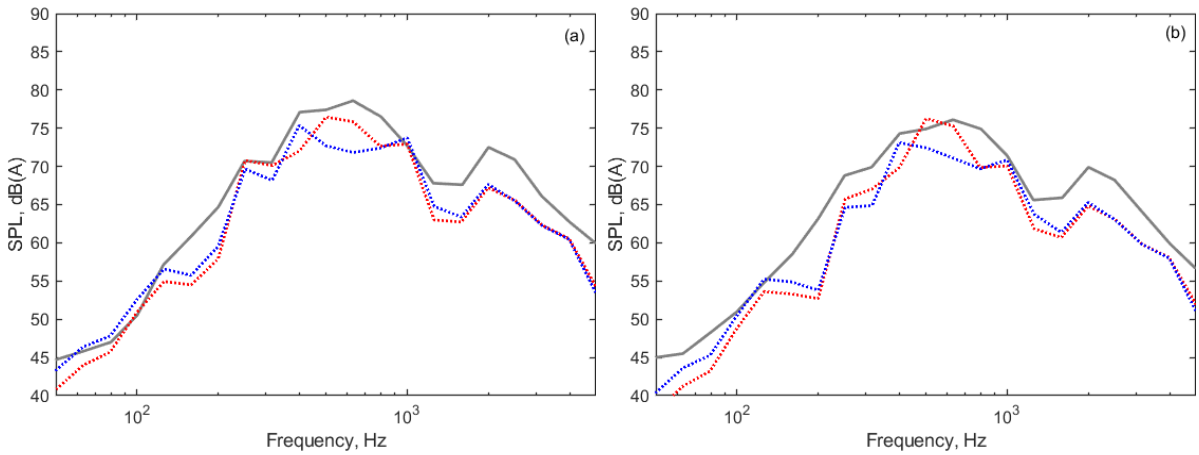

Figure 25: Comparisons between measured and predicted noise levels. (a) Averaged over receivers M1 and M2; (b) Receiver M3. —, measurement; …, TWINS prediction with continuous support; …, TWINS prediction with discrete supports.

To improve the predicted noise spectra, a correction based on the differences between the measured and predicted vibration spectra is applied to the noise calculations for the track; no correction is applied to the wheel component. Figure 26 shows the corrected noise results obtained by using the discretely supported model. The agreement with the measured results is found to be generally improved. The corrected sound powers will be used in the subsequent noise transmission calculations.

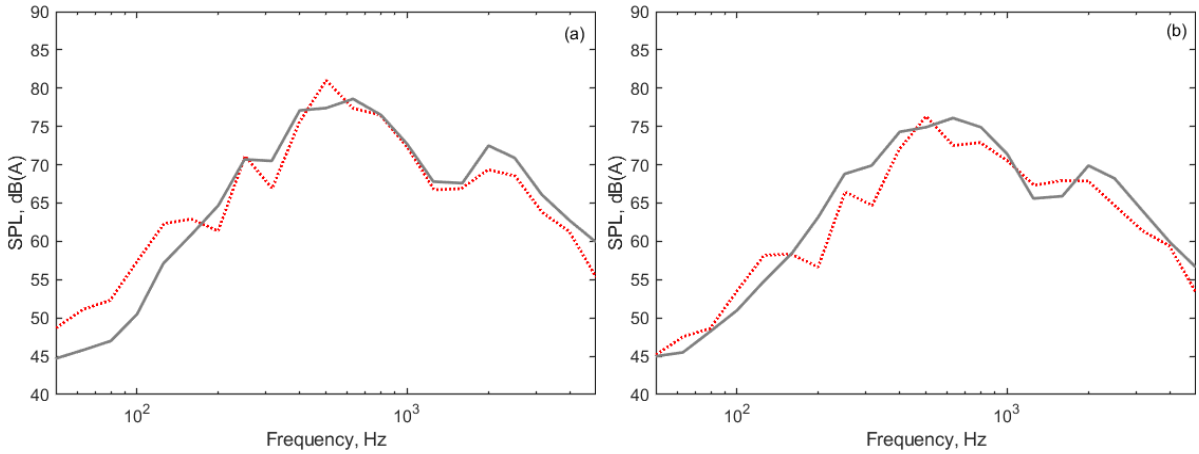

Figure 26: Comparisons between measured and predicted noise levels after correction. (a) Averaged over receivers M1 and M2; (b) Receiver M3. —, Measurement; …, TWINS prediction with discrete supports.

The sound power levels are shown in Figure 27 together with the separate contributions from the wheel, rail and sleeper. This shows that the sleeper is the dominant source up to 200 Hz and remains important up to 1 kHz due to the high rail pad stiffness. The rail, both vertical and lateral components, is dominant from 400 Hz to 2500 Hz. The wheel is only significant at 250 Hz and at 3150 Hz and above.

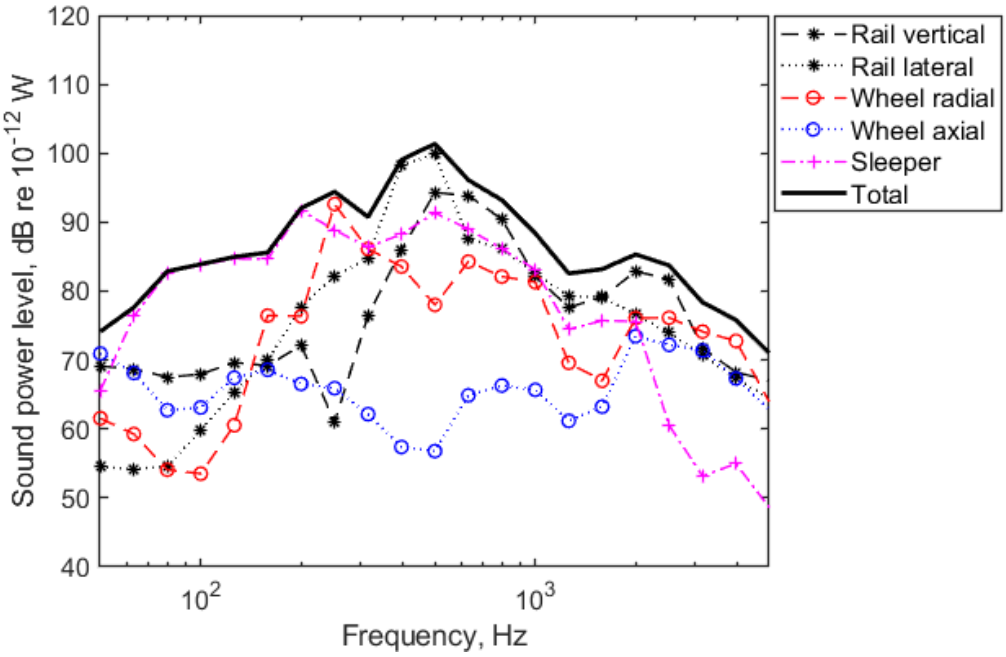

Figure 27: Sound power spectrum for one wheel and associated track vibration showing components from the wheel, rail and sleeper.

3.2 NOISE RADIATED BY THE BOGIE

The noise sources of the running gear also include the bogie frame. Due to its high rigidity, and the isolation provided by the primary suspension, the bogie frame is believed not to be a significant noise source [8]. To determine its radiated power, the three-dimensional boundary element method was used. The vibration results of the bogie frame were obtained from the Nastran model used in the structure-borne noise model described in Section 2. The velocities on the bogie surface were converted to the normal velocities and substituted into the BE model. Four load cases were calculated, consisting of unit vertical and lateral excitations applied separately on Wheels 1 and 2 (see Figure 5). Figure 28 shows the radiated powers of the bogie frame due to these unit forces. The lateral contact forces give higher radiated powers than the vertical forces for frequencies between 30 and 300 Hz. For frequencies above 300 Hz, the powers radiated by the four load cases become similar. Two dominant peaks can be observed at approximately 450 and 530 Hz for all load cases.

After the results from unit forces were converted to the 1/3 octave bands, the power radiated by the bogie frame was calculated by applying the wheel/rail contact forces shown in Figure 5. Figure 31 shows that the radiated power is lower than 50 dB below 1 kHz. Compared with the powers radiated by the wheel, rail and sleeper (as shown in Figure 27), the bogie frame radiates significantly less noise.

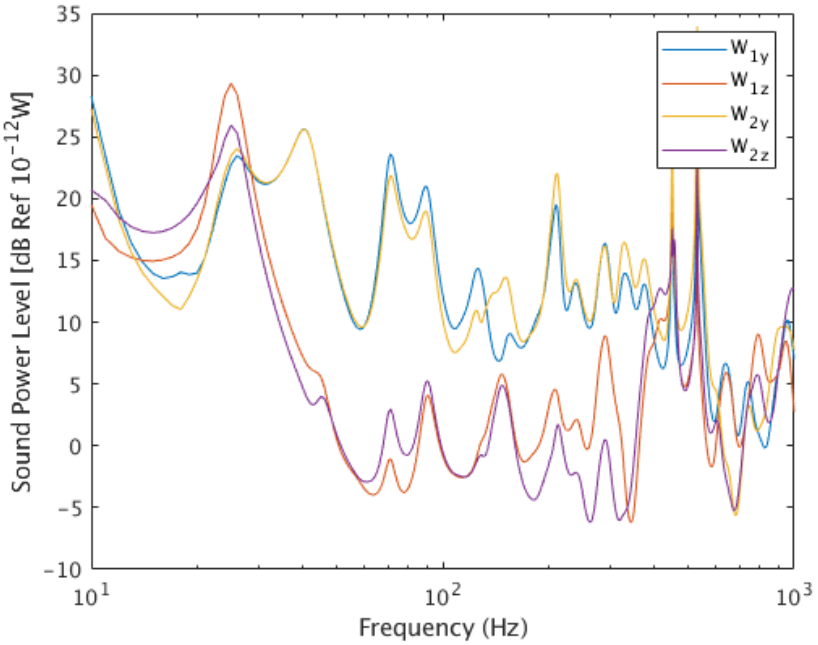

Figure 28: Sound power of the bogie frame due to unit forces at the lateral and vertical direction for wheel 1 (W_{1y}, W_{1z}) and wheel 2 (W_{2y}, W_{2z}).

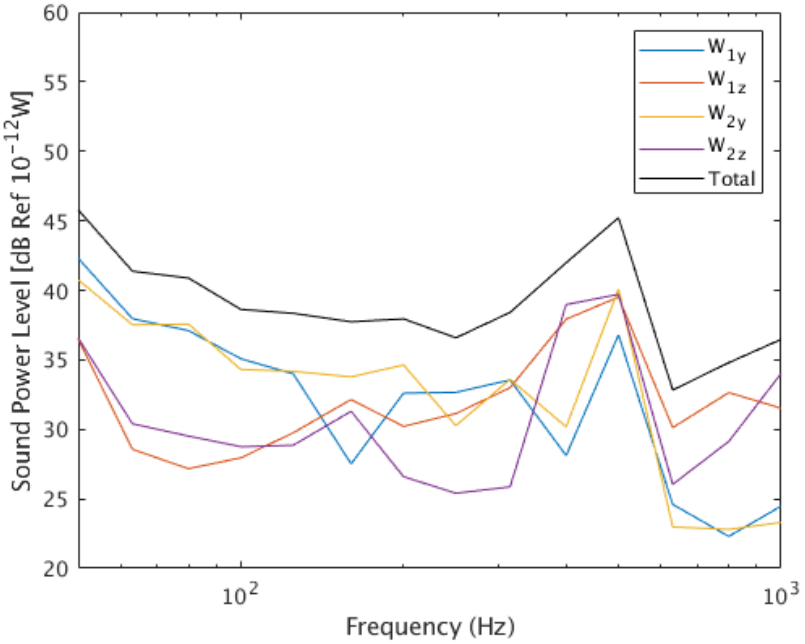

Figure 29. Sound power of the bogie frame using contact forces in Figure 5 for wheel 1 (W_{1y}, W_{1z}) and wheel 2 (W_{2y}, W_{2z}).

3.3.1 SEA model

To determine the sound pressure incident on the floor of the train a statistical energy analysis (SEA) model of the cavity beneath the train is developed. The sound pressure in this region is assumed to be sum of the direct sound from each source (wheels, rails and sleepers, from the TWINS calculations described in Section 3.1) and the reverberant sound caused by reflections from the train floor and the track. More details of the model are given in D4.2 [1].

There are fairings on the sides of the train and equipment mounted below the floor, as indicated in Figure 30. Allowance is made for these features in the definitions of the subsystem volumes and surface areas. The area below the floor is divided into eight subsystems, as shown in Figure 30(b). Subsystems 1 and 8 correspond to the region below the gangways. Due to the presence of the underfloor equipment, it is assumed that direct sound only impinges on the floor in subsystems 1, 2, 5, 7 and 8.

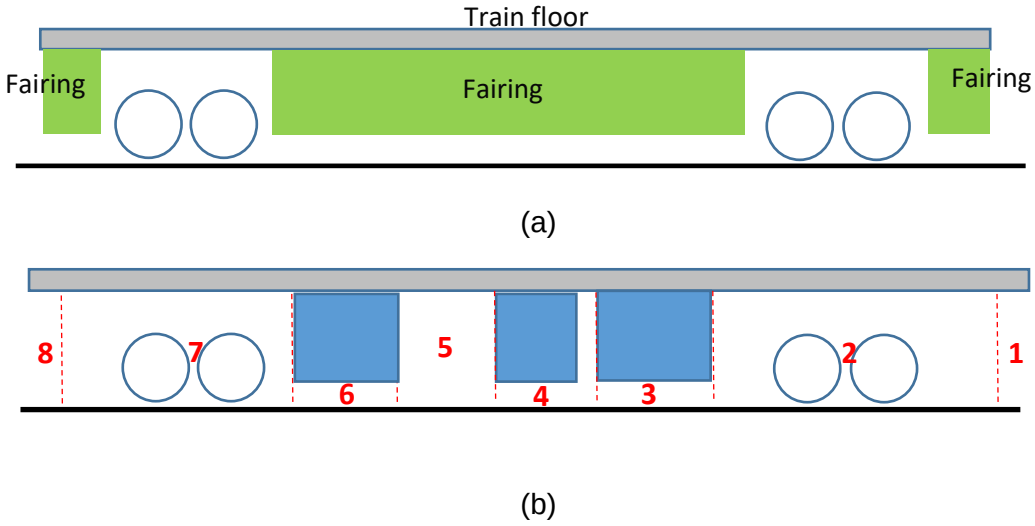

Figure 30: Schematic arrangement of (a) fairings and (b) underfloor equipment, showing division into subsystems.

3.3.2 Comparison with static measurements

Static measurements were obtained using a loudspeaker mounted under the train, as described in D4.2 [1]. The measured sound pressure levels at a height 0.32 m above the ballast are used to validate the SEA predictions. As the division into subsystems has been updated in the current

report, new results have been calculated and these are compared with the measurements in Figure 31. This shows results in example one-third octave bands between 100 and 4000 Hz; results in other bands are similar. It should be noted that these results are only used to compare the decay with distance as the source level in the measurements is unknown; the predictions have therefore been adjusted to an arbitrary level for comparison purposes. Generally good agreement is seen.

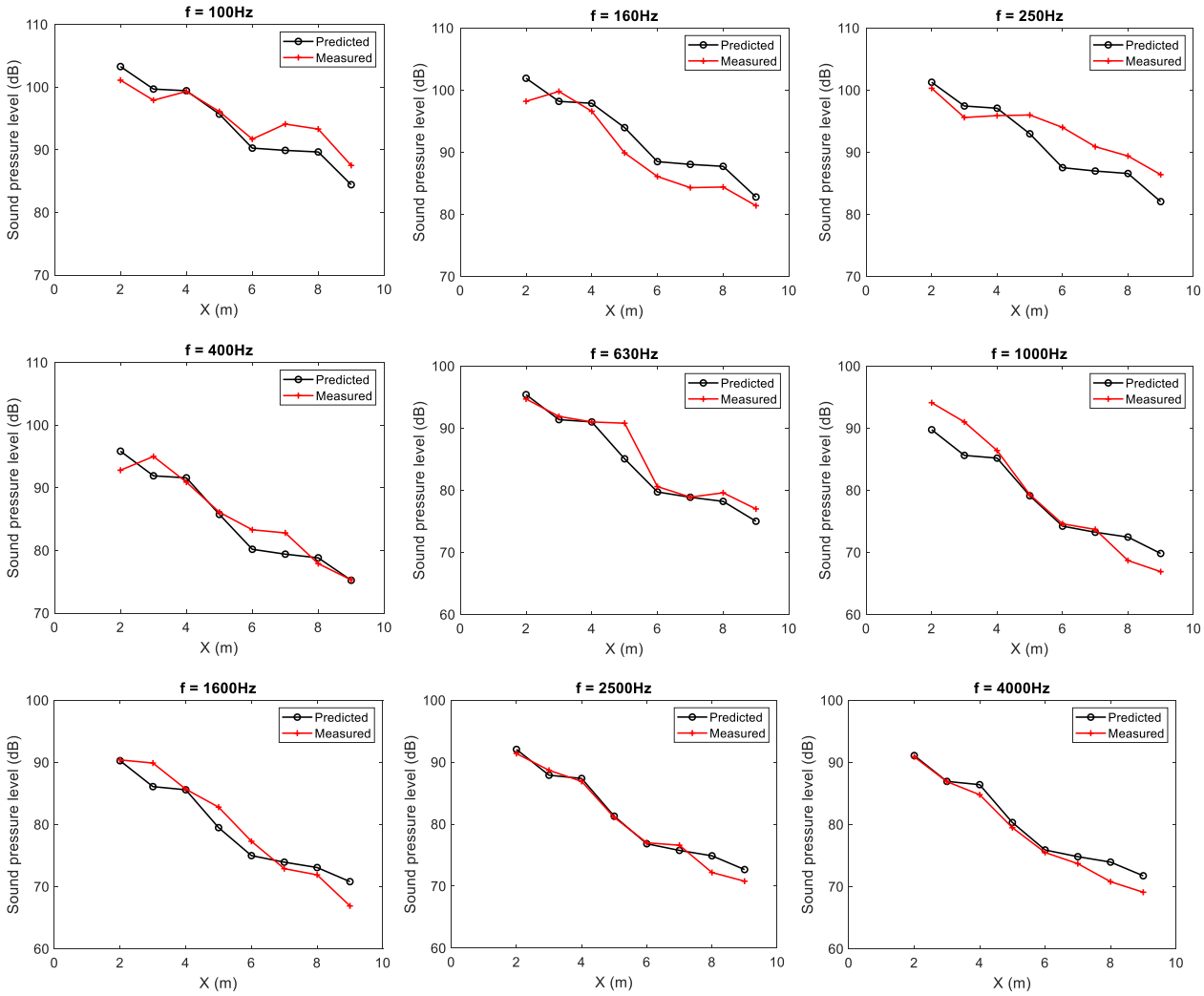

Figure 31: Comparison between measurements and predictions of noise below the vehicle plotted against distance from the loudspeaker.

3.3.3 Comparison with running measurements

During the running measurements six microphones were located below the floor, as shown in Figure 32. Point 1002 is measured below the adjacent vehicle but it is compared with predictions

at an equivalent location in segment 7 as the configuration below each vehicle is similar. The predictions of the sound pressure levels at these positions are compared with the measurements in Figure 33. The overall sound pressure levels and the differences between the predictions and the measurements are shown below in Table 6. Points 1002, 1007 and 1008 are located in the bogie area; the predicted sound pressure levels at these three positions agree well with the measurements. Points 1012 and 1013 are in the middle region below the vehicle and point 1003 is in the gangway area; the agreement at these three points is not as good as for the other three but is still acceptable. From Figure 33, it can be concluded that the differences at these three points can mainly be attributed to the overestimation of the sound pressure in the 500 Hz band.

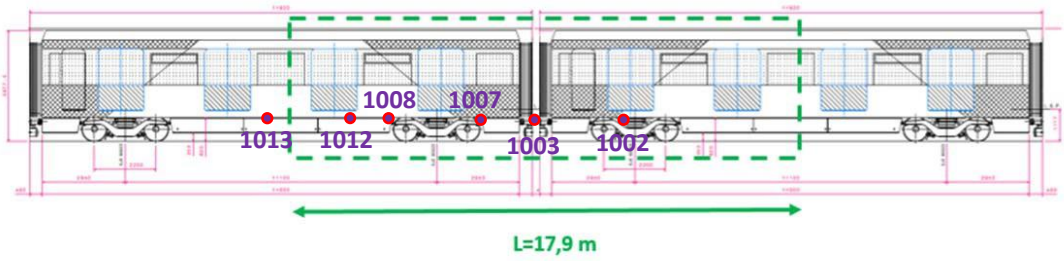

Figure 32: Microphone locations below the floor.

Table 6: Overall sound pressure levels on train floor (dB(A))

	Point 1002	Point 1003	Point 1007	Point 1008	Point 1012	Point 1013
Prediction	96.7	93.2	97.2	96.8	94.8	91.6
Measurement	96.9	90.3	96.1	94.9	92.5	89.1
Difference	-0.2	2.9	1.1	1.9	2.3	2.5

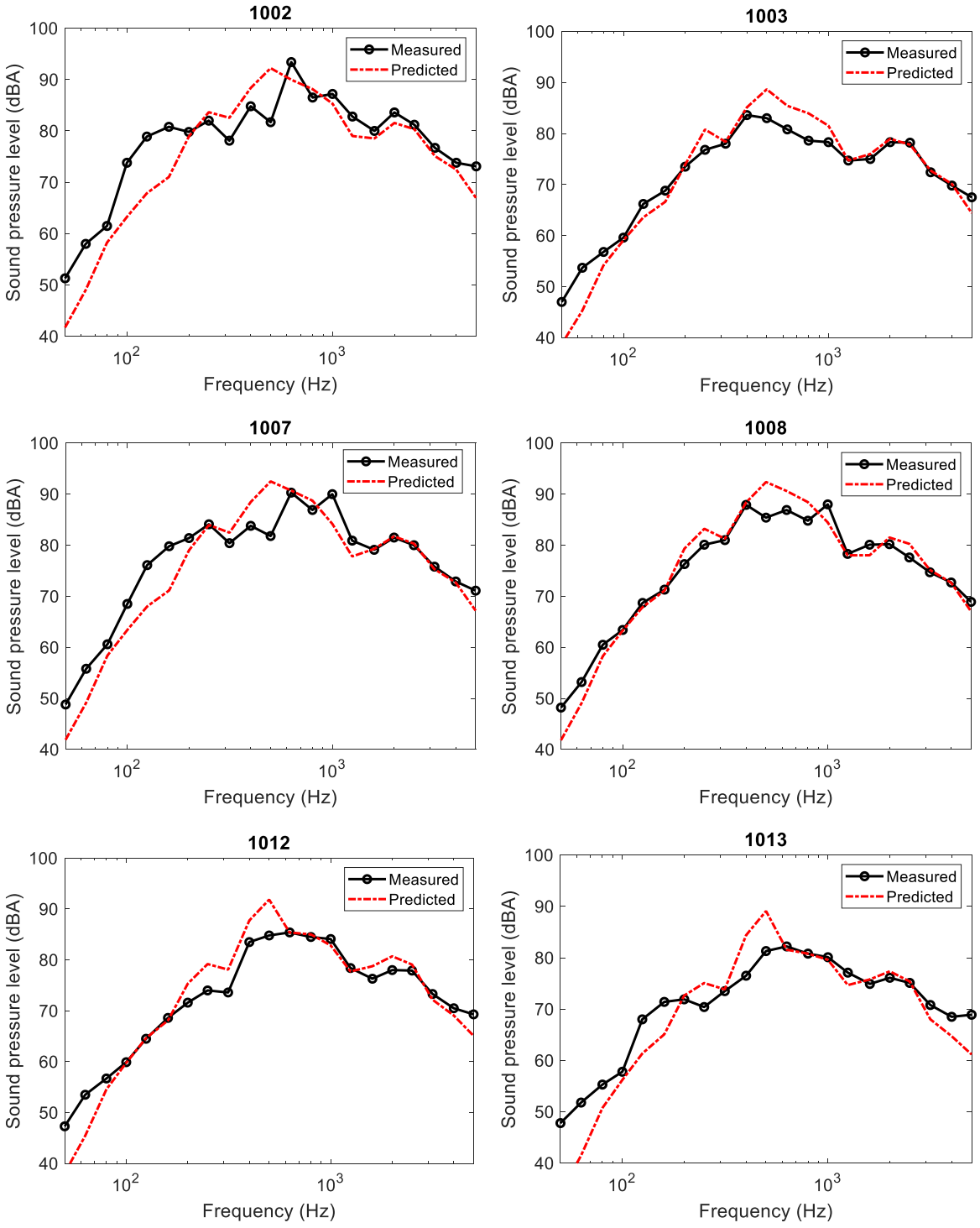

Figure 33: Comparison of predicted and measured sound pressure levels beneath the vehicle (A-weighted levels in dB re 2×10^{-5} Pa).

3.4 SOUND FIELD AT THE SIDE OF THE VEHICLE

3.4.1 2.5D BE model

The sound field on the side surfaces of the train is predicted using a 2.5D boundary element (BE) model [1]. Comparisons with static measurements using a loudspeaker source were also presented in [1].

The noise from the wheel was predicted using an average of three source heights. At each position, a monopole and a dipole are used to represent the radial and axial components of the wheel radiation. In the case of the wheel there are no fairings in the BE model of the train, see Figure 34(a). For the rail (and sleeper), vibrating surfaces are included directly in the BE model. In these cases the model includes the fairings, see Figure 34(b). Altogether the noise from 8 wheelsets (16 wheels) and two rails is included. The noise from each source is added considering them to be incoherent.

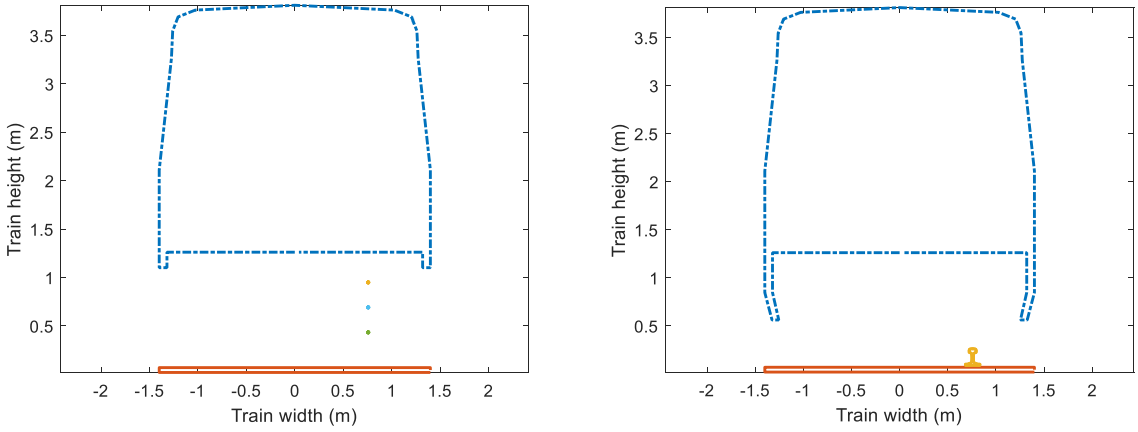

(a) (b)

Figure 34: 2.5D boundary element model of the train. (a) Wheel sources; (b) rail source.

3.4.2 Comparison with running measurements

During the field measurements the sound pressure was measured on the external train surfaces in running operation at 50 km/h. Four microphones were located above the bogie area, as shown in Figure 35. Microphones 1006, 1009, 1011 are 0.7 m above the bottom edge of the sidewall and microphone 1010 is 1.5 m above it. In addition two microphones were located in the gangway area at different heights, numbered as points 1004 and 1005.

Figure 35: Microphone locations on the side of the train.

The predicted noise levels on the side wall are compared with the measurements in Figure 36. The corresponding results for the two positions at the gangway are shown in Figure 37. The overall sound pressure levels from the predictions and the measurements, together with the relative error between them, are listed in Table 7. The comparisons show that the 2.5D model is able to predict satisfactorily the sound pressure on the train external surfaces during running operation. As with the noise under the floor, the prediction is too high in the 500 Hz band. It is also too high at high frequencies but lower than the measurements at frequencies below 200 Hz.

Table 7: Overall sound pressure levels on train sides (dB(A))

	Side wall				Gangway	
	Point 1006	Point 1009	Point 1010	Point 1011	Point 1004	Point 1005
Prediction (dB(A))	83.1	83.1	80.7	82.9	82.6	80.2
Measurement (dB(A))	80.6	81.1	78.3	80.4	83.2	80.9
Difference (dB(A))	2.5	2.0	2.4	2.5	-0.6	-0.7

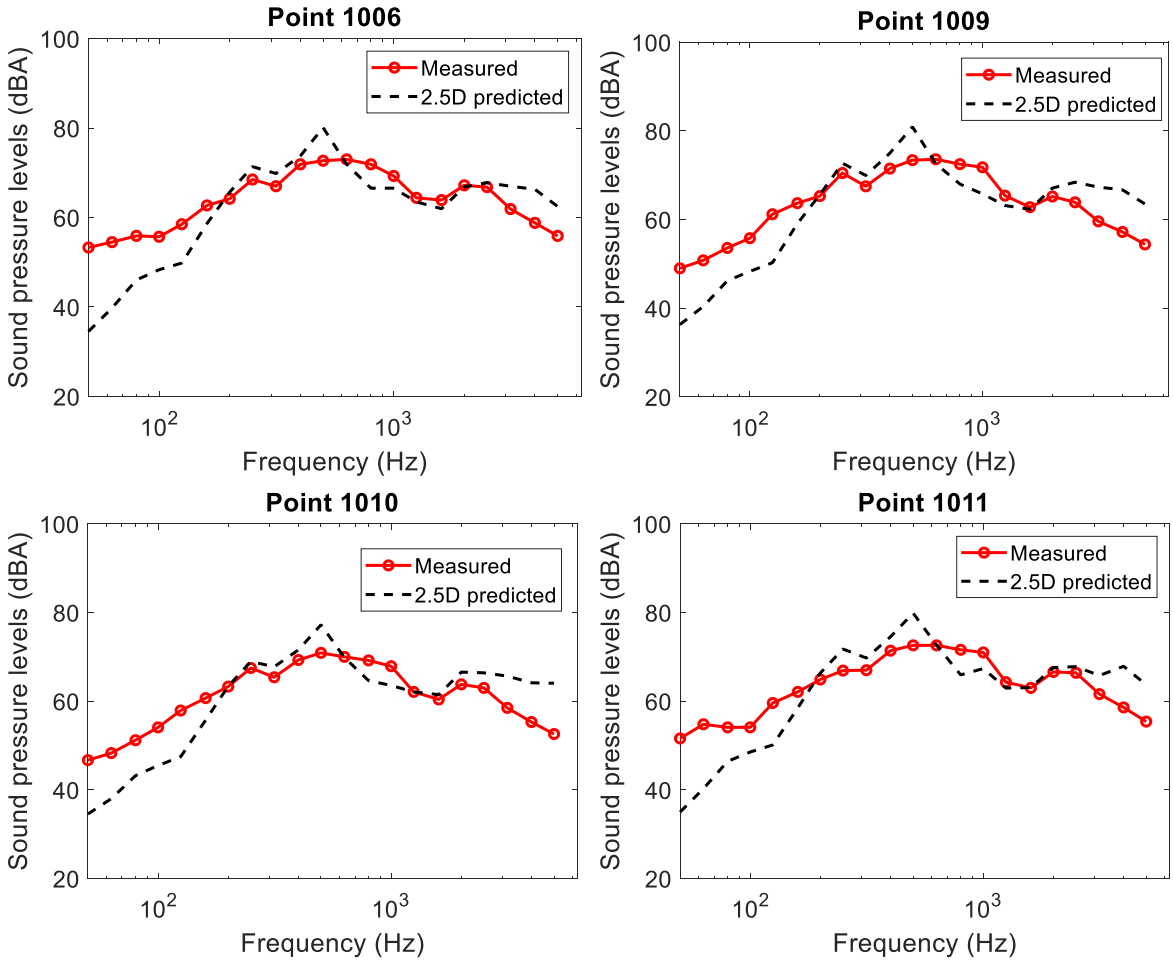

Figure 36: Comparison of predicted and measured sound pressure levels on the external side of the vehicle (A-weighted levels in dB re 2×10^{-5} Pa).

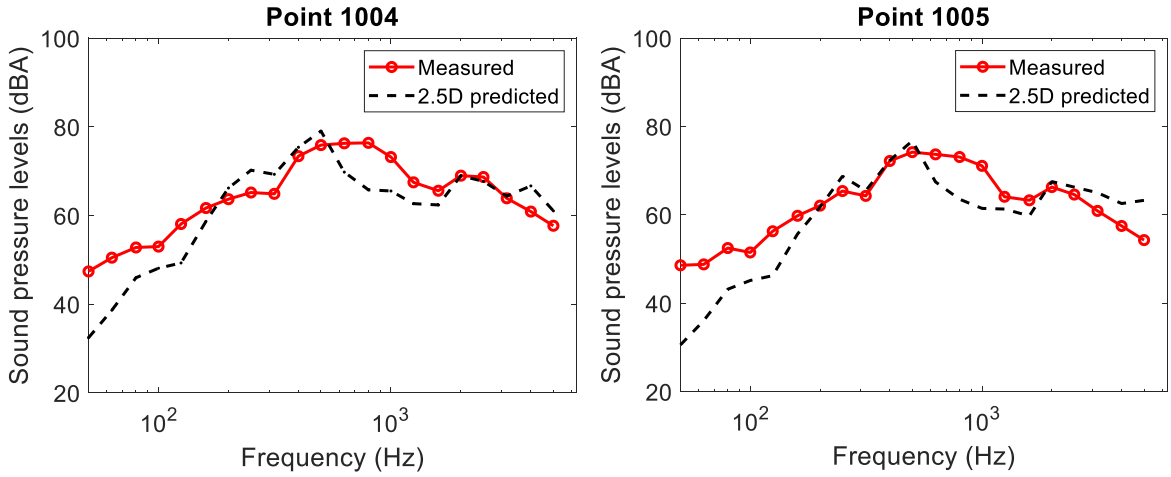

Figure 37: Comparison of predicted and measured sound pressure levels on the side of the gangway region (A-weighted levels in dB re 2×10^{-5} Pa).

3.5 AIRBORNE SOUND INSIDE THE VEHICLE

To predict the interior noise, an SEA model has been created for the interior region. The subdivision of the interior is based on the configuration of the train body structure. According to the location of the doors and windows the vehicle is divided into 9 segments; another two subsystems are created to model the gangway regions. The subdivision of the interior region and the train side surfaces is shown in Figure 38.

The sound power transmitted into the vehicle is determined from the exterior sound pressure spectra in combination with measured transmission loss spectra for various components of the train car body. The absorption in the train interior is also required and was determined from the measured reverberation times given in [1].

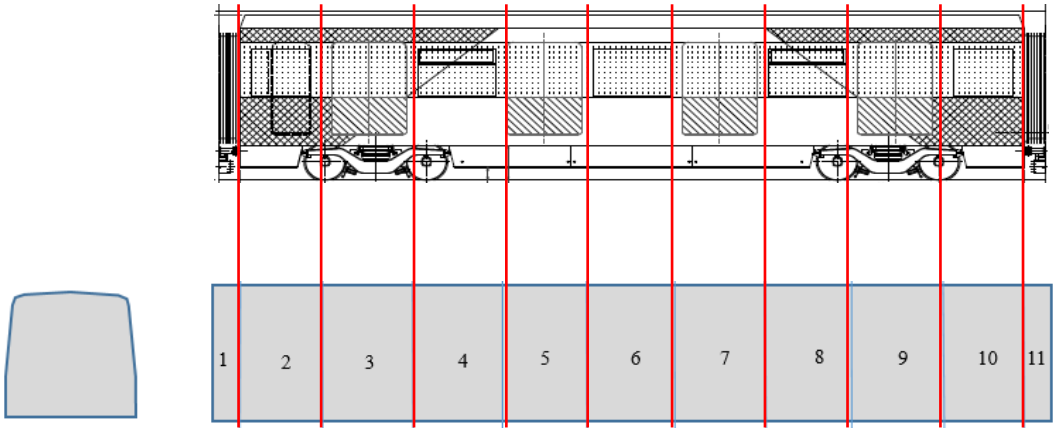

Figure 38: Subdivision of the train sides and interior area into SEA subsystems.

During the field measurements the sound pressure was measured inside the vehicle for a running speed of 50 km/h. Four microphones were located inside the vehicle, named as points 2003 to 2006, and one in the gangway, named as point 2002. Their locations are indicated in Figure 2.

The predictions of the sound inside the vehicle obtained from the SEA model are compared with the measurements in Figure 39 and the differences in overall A-weighted levels are given in Table 8 (absolute levels are not shown for confidentiality reasons). Reasonable agreement is obtained although there is a consistent over-prediction at 500 Hz and an under-prediction at high frequencies; the overall level is over-predicted by 2-3 dB.

Table 8: Difference in overall sound pressure levels inside the train (dB(A))

	Point 2002	Point 2003	Point 2004	Point 2005	Point 2006
Prediction – Measurement (dB(A))	2.1	2.8	3.2	2.9	2.9

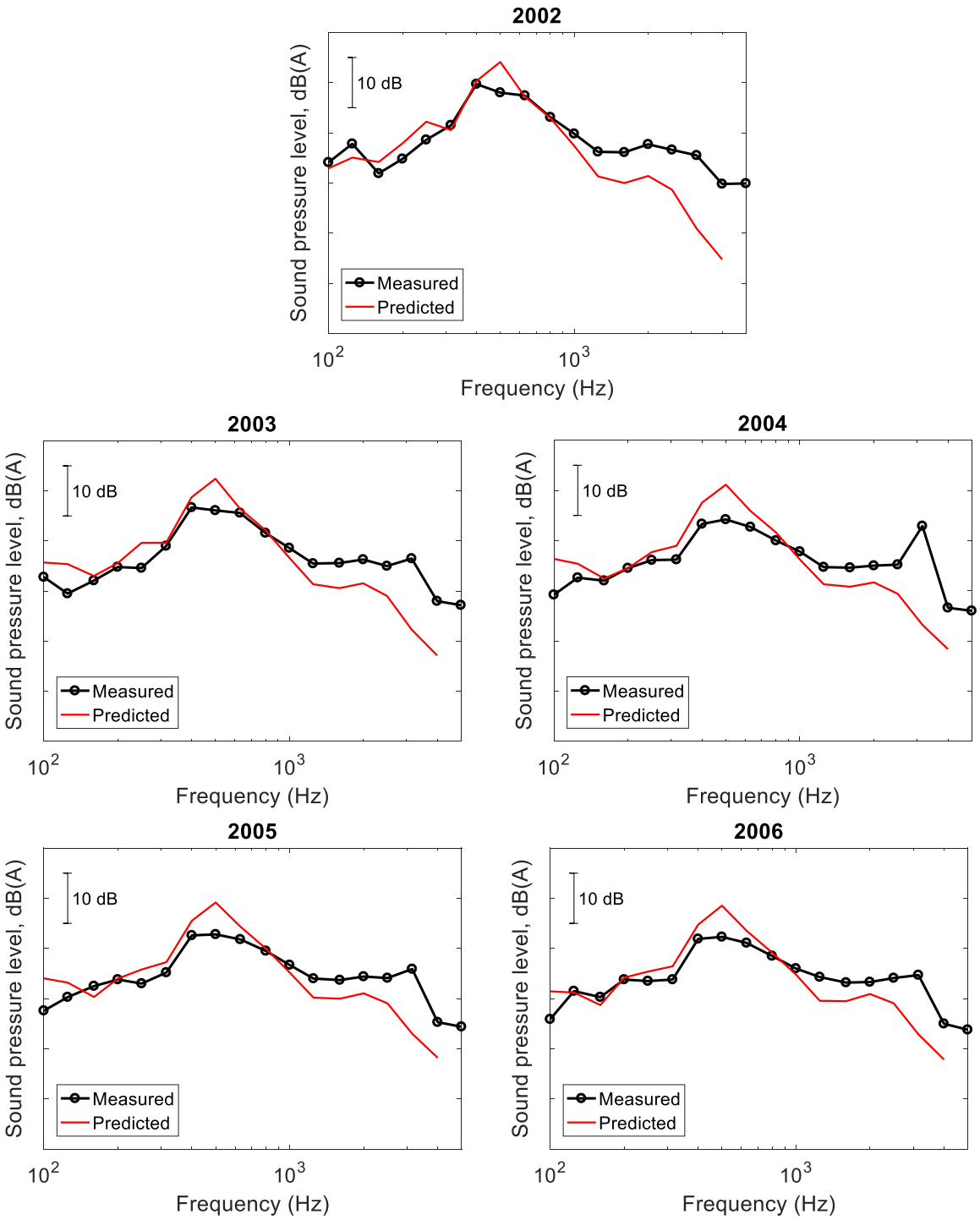

Figure 39: Comparison between measured and predicted noise inside the vehicle.

The sound power incident on the train sides, floor and gangway area are calculated separately, and shown in Figure 40(a). The largest power is incident on the floor as it is nearest to the source. The power incident on the sides and the gangway are similar (the gangway area is smaller but it has direct sound whereas for the sides the sound is attenuated). The sound power transmitted through the three components is shown in Figure 40(b). The gangway has the lowest sound transmission loss, so the largest component of the power transmitted into the train cabin comes from the gangway region for frequencies above 250 Hz.

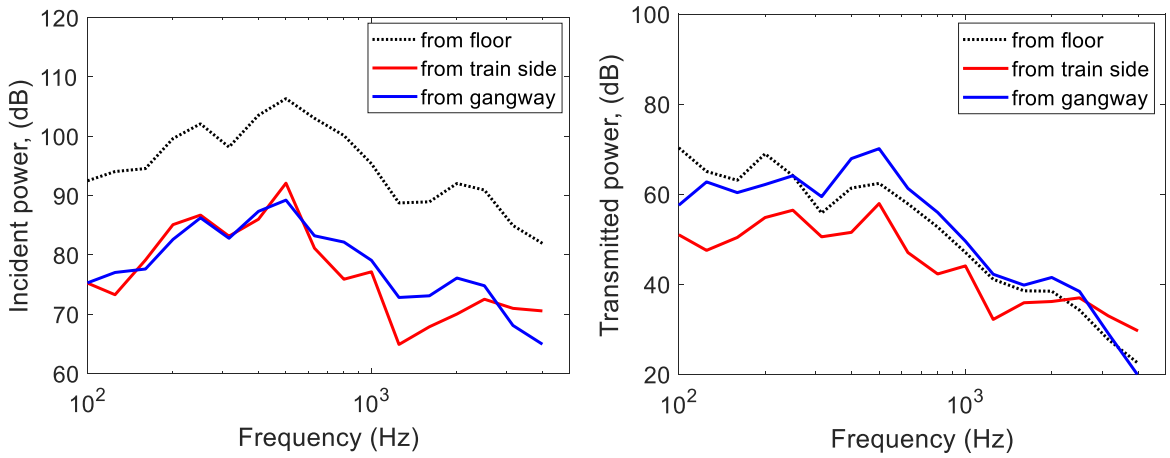

(a) (b)

Figure 40: Sound power (a) incident on different surfaces and (b) transmitted through different surfaces to the inside the vehicle.

4. CONCLUDING REMARKS

4.1 GLOBAL SUMMARY

Figure 41 presents the computed contributions of airborne and structure-borne transmission paths in the frequency range [100, 5000] Hz. A reasonable agreement between computed and measured noise is achieved, with an over-prediction of around 3.2 dBA for the overall interior noise in this range (see Table 9). Note that the over-prediction at 500 Hz by about + 6dBA is the main reason for the global over-prediction. The peak is related to the very particular behaviour of the test track. On more conventional tracks this overestimation should not occur.

The key points of the work carried out in Tasks 4.3, 4.4 and 4.5 of WP4 are the following:

- For structure-borne noise: development and validation of a new methodology for structure-borne transmission, from wheel rail-contact force to interior noise, based on existing FE models.
- For airborne noise: development and validation of new methodologies to compute the exterior sound field around the train, based on an SEA model for under-floor propagation, and 2.5D BEM model for propagation towards the lateral sides of the train.
- Each of these methodologies presents a good compromise between accuracy and effort and may thus be of significant interest to rolling stock manufacturers.

The following sections summarize the structure-borne and airborne noise methodologies their main results and the possible areas of improvement.

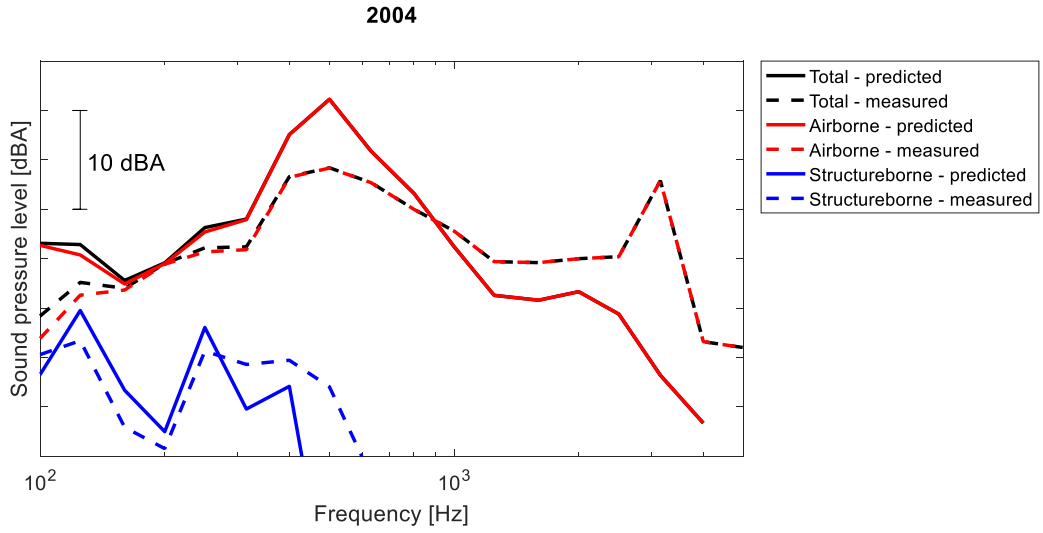

Figure 41: Computed airborne and structure-borne contributions (microphone 2004)

Table 9: Difference in overall sound pressure levels inside the train (microphone 2004, range: 100-5000 Hz)

	Airborne	Structure-borne	Total
Prediction – Measurement (dB(A))	3.2	0.5	3.2

4.2 STRUCTURE-BORNE NOISE MODEL

A new methodology for structure-borne noise prediction has been implemented and validated against field test results. This methodology is based on the following steps:

- Construction of a complete bogie FE model including wheelsets, bogie, suspension elements, traction bars and dampers. A particular feature is that all suspension elements and rubber bushings are modelled using spring-damper elements with optionally frequency-dependent properties. Note that:
    - The carbody is not included in this model as it was not available for the project: it is replaced by a clamped boundary condition at the carbody connecting points with traction bars and dampers. However, the method can be extended to include a carbody model.
    - The FE model was taken “as it is” without any particular tuning. Only global parameters like damping were tuned in order to fit to measured data.
- This model is used to compute FRFs between unit contact forces at wheel/rail interface and blocked forces transmitted to the carbody. A specific modal solver, taking into account frequency dependent stiffness, has been validated to speed-up computation time.
- A specific post-processing algorithm which combines contact forces with the complete bogie FRFs has been developed. The outputs are the operating acceleration levels and blocked forces on the carbody. These blocked forces are then multiplied by the carbody vibro-acoustic transfer functions p/F to estimate the structure-borne noise contributions.

This computed structure-borne contribution has then been validated by comparison with test results (TPA analysis). Despite high uncertainties on several input parameters (roughness for long wavelengths, track receptance, no tuning of the FE model), the comparison with measured data is satisfactory:

- Above the bogie where structure-borne noise is more significant; the global structure-borne noise levels are predicted with an accuracy between 1 to 3 dBA, depending on the measurements points and the frequency bandwidth which is considered.
- In terms of 1/3 octave band spectra, the agreement is very good between 80 and 400 Hz. Above 500 Hz, the structure-borne noise contribution is strongly under-predicted (but at these frequencies airborne contribution is already predominant).
- A detailed investigation of the individual transfer paths reveals that the contribution of the traction bars is under-estimated, whereas the contribution from the lateral dampers is correctly predicted.

These first results are encouraging and confirm the feasibility of the chosen approach. In order to improve the predictions, the following directions for improvement are identified:

- Global bogie FE model: Tuning to the static measurements (damping, modes, …) and a more accurate modelling of the traction bars and lateral dampers (currently simple beam elements),
- Input parameters: reduction of the uncertainties related to parameters such as roughness and track receptance.
- Frequency-dependent stiffness: More reliable data of the rubber bushings at the extremities of the traction bars and dampers as their vibration filtration effect is currently over-estimated.

Finally, the new method to predict structure-borne noise has proven its applicability and can thus be used in industrial applications. Even if absolute levels are hard to predict and require some effort, the method gives efficient access to identifying critical transmission paths, to impacts of different operational conditions and to effects of bogie design modifications.

Furthermore, the method could be integrated easily in the railway industry's work scheme and capacity, since it can rely on existing FE models, with very reasonable FE model size (about 4 million DOF) and computation time (between 30 min and 2 hours depending on the computer). It enables sub-component teams (e.g. bogie and carbody) to work independently: the bogie team can, for example, focus on blocked forces whereas the carbody team remains responsible for the interior acoustic performance of the vehicle.

4.3 AIRBORNE NOISE MODEL

A global method has been developed to determine the airborne noise transmission by predicting the noise radiated by the wheels, track and bogie frame and its transmission to the exterior sound pressure on the surface of the car body.

A TWINS model has been implemented to estimate the rolling noise sound power. Because of the large sleeper spacing (1 m) at the test track, a discrete support track model has been used to improve the comparison with measurements. Based on the remaining difference between the predicted and measured rail vibration, a correction is determined and applied to the predicted noise results. The corrected sound power has been used in the subsequent noise transmission calculations.

The acoustic radiation by the bogie frame is generally neglected for interior / exterior noise predictions, due to a lack of input data. In order to confirm this assumption, a BEM model has been implemented, using as a starting point the bogie FE model developed for structure-borne noise computations: the normal velocities of the bogie frame are introduced into the BE model to compute its sound radiation. It is found that the bogie frame radiates significantly less noise than by the wheel, rail and sleepers, and can effectively be neglected for interior/exterior noise computations.

For industrial applications, the determination of the exterior sound field around the coach is always a difficult step. Several computation methods have previously been tested (3D BEM, ray-tracing, SEA, …) but none of them has imposed itself, either because of accuracy and/or because of prohibitive computational time. Consequently, experimental databases of acoustic transfer functions measured with artificial sources at standstill or in rolling conditions on similar coach geometries are still used, with the main drawback that for new rolling stock geometry it is difficult to transpose them from one vehicle to another.

Two separate models have been implemented for RUN2Rail project:

- An SEA model of the under-floor cavity has been developed to obtain sound pressure levels at the train floor. This model has been validated by comparison with static tests with a loudspeaker and with rolling tests.
- Through reflections and diffraction, noise also reaches the lateral sides of the train. An original 2.5D boundary element model has been developed for this. The comparisons with measurements show that this model is able to predict satisfactorily the sound pressure on the train external surfaces during running operation, with differences between computed and measured pressure levels of about 2 – 2.5 dBA.

For these two types of model, the compromise between the accuracy and the short computation times is very promising for further railway industrial applications.

For interior noise, an SEA model has been developed. The injected acoustic powers to the interior cavity are computed from the exterior acoustic loading of panels (floor, doors, windows, lateral sides, gangway) and panel transmission loss (which are obtained from in situ measurements). This type of modelling approach is very classical in industrial applications. Reasonable agreement with measurment is obtained; the overall level is over-predicted by 2-3 dB.

REFERENCES

[1] D.J. Thompson et al. Complete virtual test method for structure-borne and airborne noise transmission. RUN2Rail Deliverable D4.2, March 2019.

[2] I. Lopez Arteaga et al. Description of methods for characterizing suspension elements. RUN2Rail Deliverable D4.1, December 2018.

[3] D.J. Thompson, B. Hemsworth and N. Vincent. Experimental validation of the TWINS prediction program, part 1: description of the model and method. Journal of Sound and Vibration 193, 123-135, 1996.

[4] D. Thompson. Railway noise and vibration: mechanisms, modelling and means of control. Elsevier: Oxford, 2009.

[5] X. Zhang, G. Squicciarini, D.J. Thompson. Sound radiation of a railway rail in close proximity to the ground, Journal of Sound and Vibration. 362, 111-124 (2016).

[6] X. Zhang, D.J. Thompson, G. Squicciarini. Sound radiation of railway sleepers, Journal of Sound and Vibration. 369, 178-194 (2016).

[7] ISO 3095, “Railway applications – Acoustics – Measurements of noise emitted by railbound vehicles”, International Standards Organization, Geneva, 2013.

[8] F. de Beer and J.W. Verheij, Experimental determination of pass-by noise contributions from the bogies and superstructure of a freight wagon, Journal of Sound and Vibration 231, 639-652, 2000.

APPENDIX A: RUNNING MEASUREMENTS

A.1 ACCELEROMETER INSTRUMENTATION PLAN

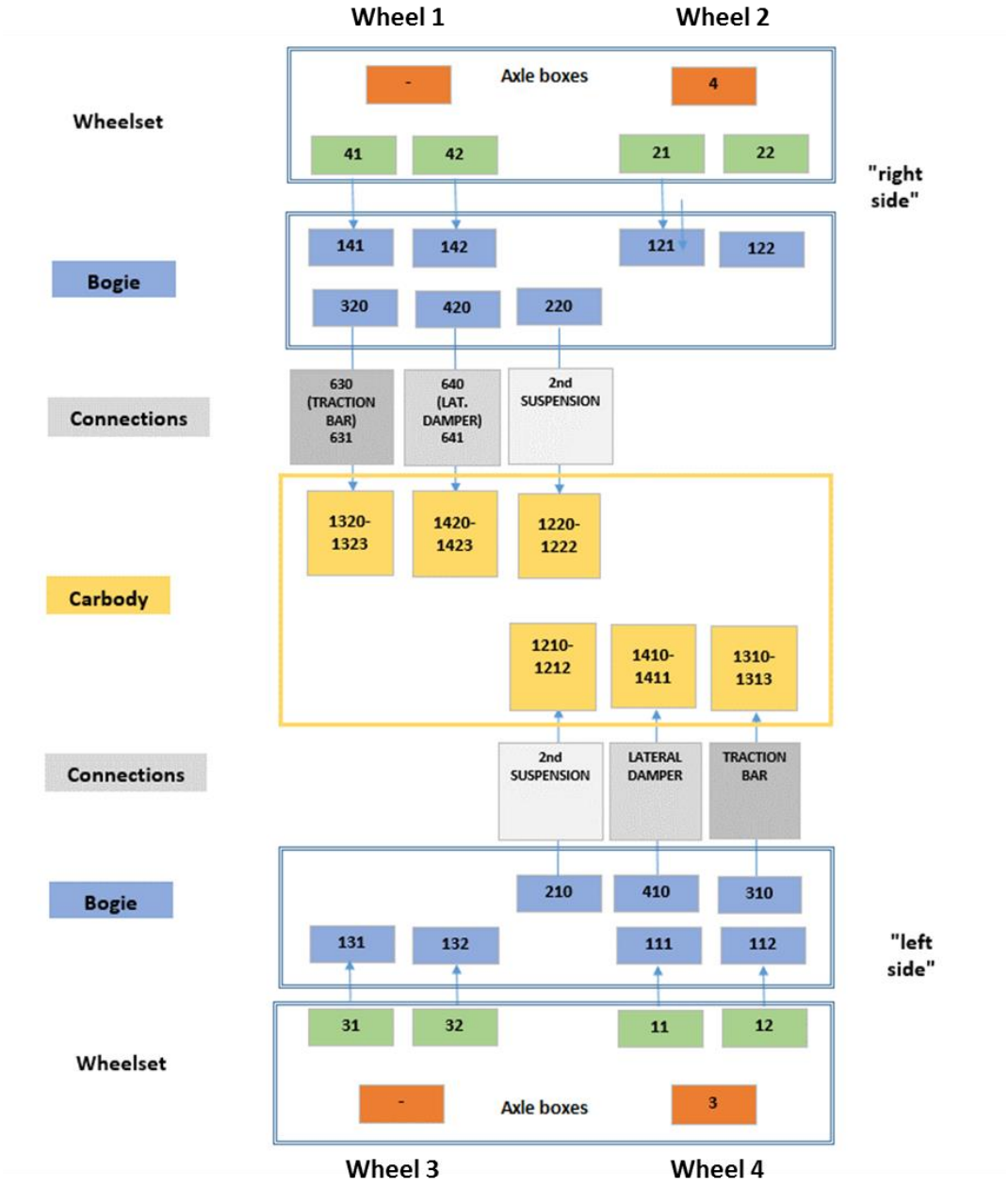

Figure 42: Accelerometer instrumentation plan for dynamic tests

A.2 PASS-BY NOISE MEASUREMENT

Figure 43 shows the microphone locations for the pass-by noise measurements. Measurement data is centred on the trailer bogie under investigation. The power to the adjacent motor bogie was switched off during measurements.

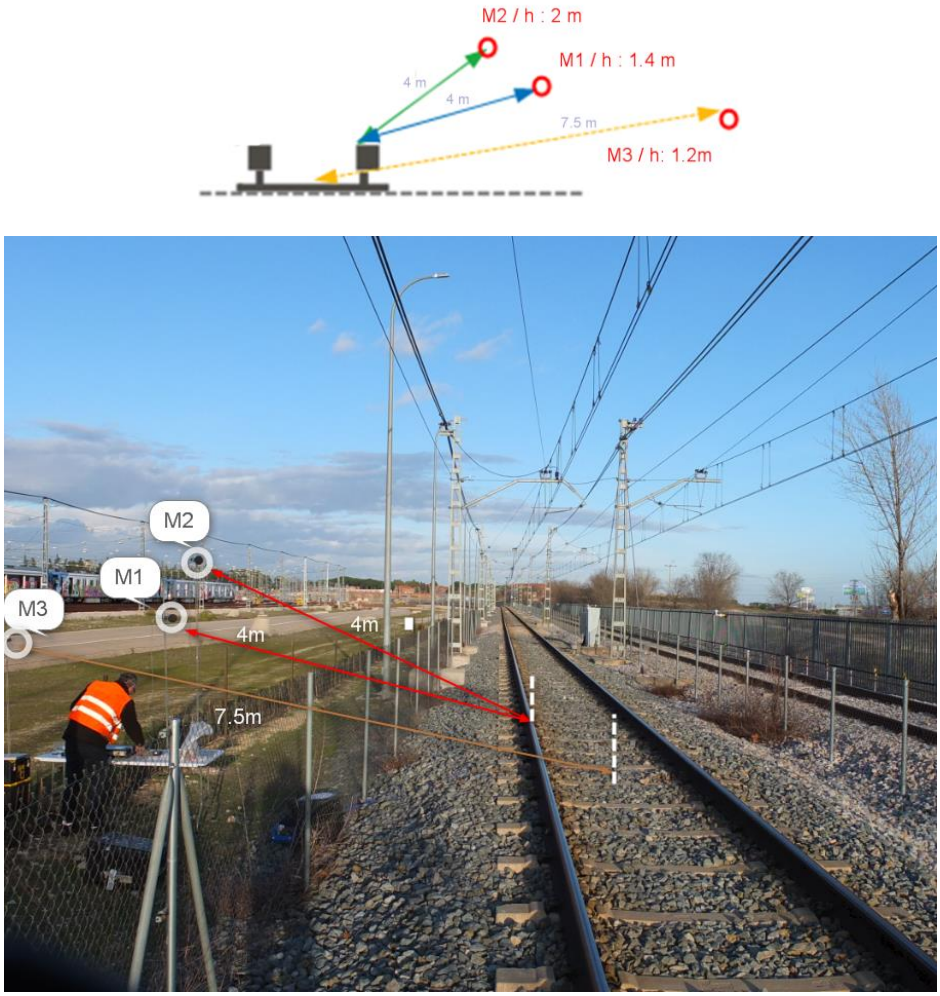

Figure 43: Pass-by noise microphones: M1 and M2 at 4 meters from the rail head, M3 at 7.5meters from the centreline of the track